Gamma-ray and Neutrino Emission in X-ray binaries: The Role of Jet Cooling, Photo-absorption, and Black Hole Spin

Theodora Papavasileiou, Ph.D.

Department of Physics, University of Ioannina, Greece

Department of Informatics, University of Western Macedonia, Greece

Neutrinos Electro-Weak interactions and Symmetries

Colloquium

NEWS

July 18th, 2025

University of Ioannina

UNIVERSITY OF WESTERN MACEDONIA

Outlook

- Introduction – X-ray Binary systems (XRBs)
- Accretion disk and XSPEC models
- Detection of cosmic neutrinos & VHE γ-rays
- Emission from relativistic jets: (i) Leptonic emission mechanisms, (ii) Hadronic interactions
- Results – High-energy gamma-rays and neutrinos from XRBs
  - Q: Can photo-absorption and particle cooling explain the lack of VHE observations?
  - Q: What is the jet configuration comprising an optimized particle accelerator?
- Results – Calculating relativistic disk spectra
  - Q: Is there a simpler and more time-conserving way to obtain relativistic spectra from accretion disks?
- Summary & conclusions

I. Introduction

What are X-ray Binary systems?

Systems consisting of a **compact object** (black hole or neutron star) devouring mass out of its **stellar companion**

- **Accretion disk**: forms out of the companion's mass at the equatorial plane
  - Some of the brightest X-ray emission sources in our Galaxy
  - Temperature of $\sim 10^6 - 10^7$ K near the black hole
  - Size $10^6 - 10^{11}$ cm & luminosity $L < L_{Edd} \approx 10^{39}$ erg/s

- **Relativistic jets**: plasma ejections perpendicularly to the disk
  - Collimated and accelerated by the system's magnetic field
  - Form observable radio lobes at distances $\sim 10^{17}$ cm
  - Powerful particle accelerators

- **Corona**: spherical plasma region around the black hole
  - Consists mainly of thermal electrons
  - Up-scatters photons from the disk

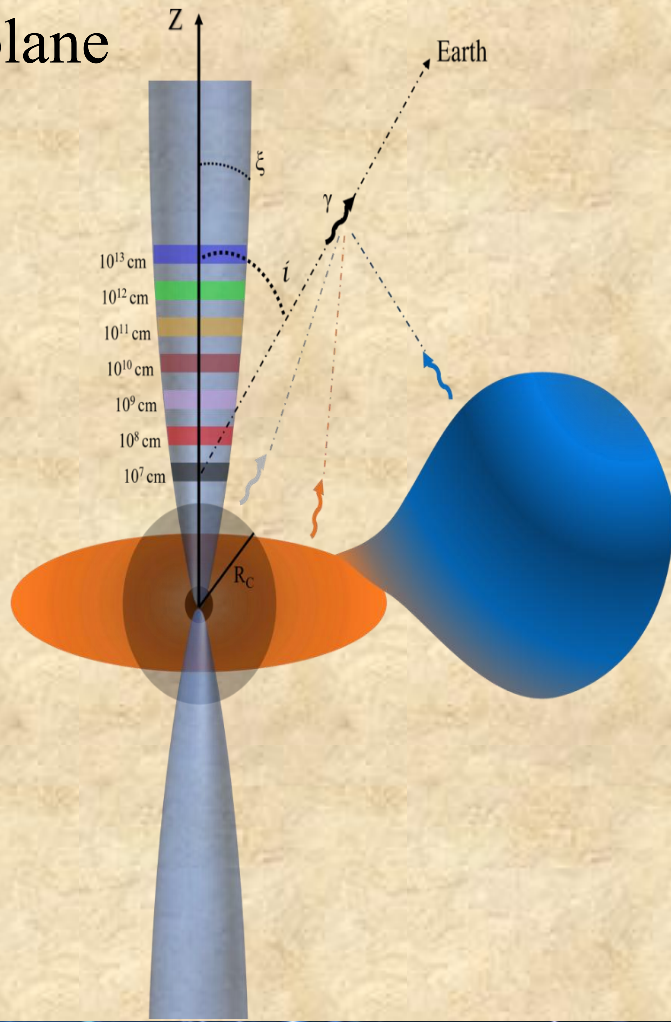

Why X-ray binaries?

- **Similarities to AGNs**: XRBs are scaled-down galactic centers featuring supermassive BHs
  - Some of the most luminous objects in the Universe
  - Accelerate the most energetic cosmic rays reaching the Earth
  - Offer significant insights into the evolution of the Universe

  But with:
  - Much smaller distance than the nearest AGNs
  - Much shorter evolution timescale

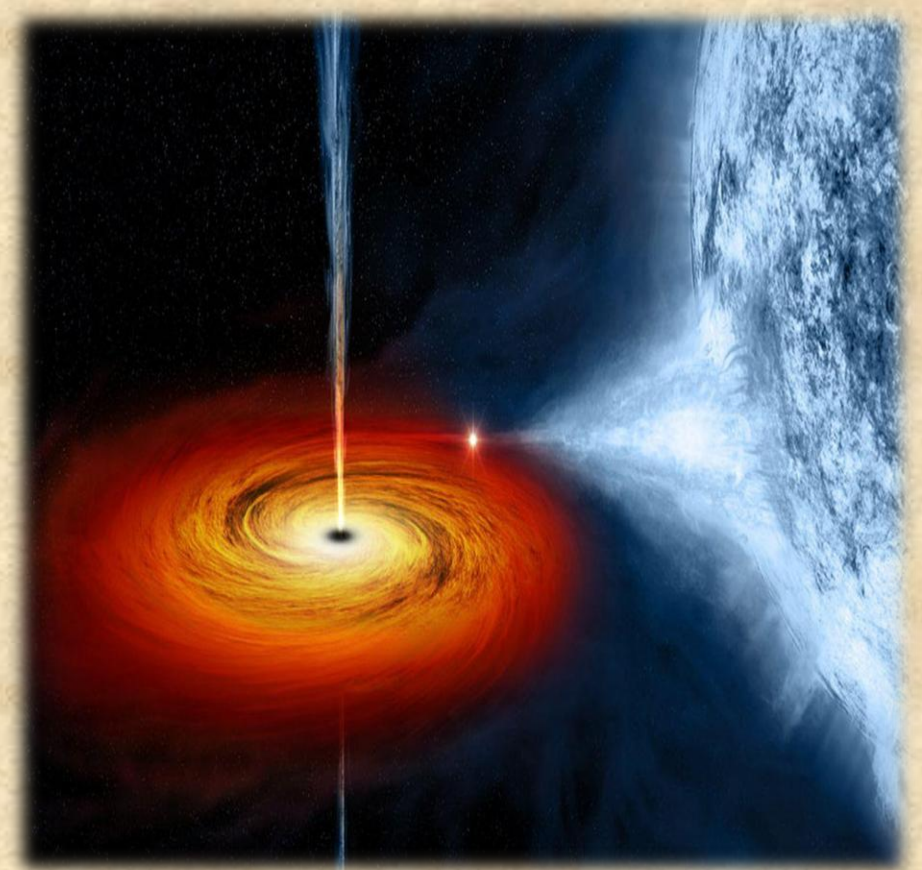

- **Providing valuable insights on**:
  - The black hole including its mass, spin, and evolution
  - The jet collimation and acceleration mechanisms
  - The accretion process and formation of the disk
  - The transition between different spectral states
  - The disk-corona dynamics

II. Accretion disk models

Accretion Disk-Thin Disk Models

ADAF	Shakura-Sunyaev "Standard" disk	Slim disk
• Sub-Eddington accretion, small opacity • Very radiatively inefficient • Cooled by advection instead of radiation • Sphere or "corona"-like shape • $R_{in} < R_{ISCO}$	• Very sub-Eddington accretion, very high opacity • High luminosity, high efficiency of radiative cooling • Keplerian rotation • Spectra similar to a sum of black-bodies • Dynamically stable • $R_{in} = R_{ISCO}$ • The best known and studied theoretical model	• Nearly Eddington accretion, large opacity • Radiatively much less efficient than the "Standard" disk • Cooled by advection and radiation • Slightly different than Keplerian rotation • Dynamically, thermally and viscously stable • $R_{in} < R_{ISCO}$

$\longrightarrow \dot{M}/\dot{M}_{Edd}$

Emission from the Accretion Disk

Shakura-Sunyaev "Standard" disk

- Angular velocity

$$\omega = \left(\frac{1}{r}\frac{d\Phi}{dr}\right)^{1/2}$$

- Surface brightness

$$F = \frac{-\dot{M}(j - j_0)}{4\pi r}\frac{d\omega}{dr}$$

- Disk temperature profile

$$T(r) = \left(\frac{F}{\sigma}\right)^{1/4}$$

- Emitted photon density

$$\frac{dn}{d\Omega d\epsilon} = \frac{2}{h^3c^3}\frac{\epsilon^2}{e^{\epsilon/kT(r)} - 1}$$

III. Detection of cosmic neutrinos & VHE γ-rays

Detection

Neutrino observatories

- **Super-Kamiokande (Super-K)** is one of the most important and influential neutrino detectors in the world
- **Location**: 1 km under Mt. Ikenoyama, Gifu Prefecture, Japan
- **Sensitivity**: 10 MeV to a few hundred GeV

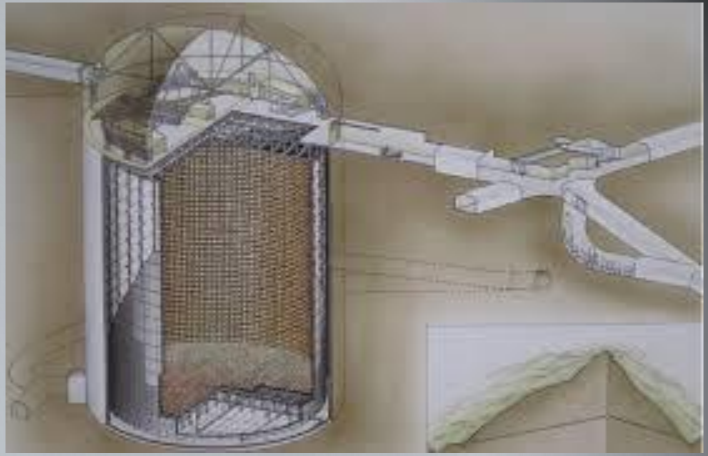

- **KM3NeT** is the European counterpart to the IceCube Neutrino Observatory at the South Pole
- **Location**: 2.5–3.5 km below sea level, Mediterranean Sea, Offshore Capo Passero, Sicily (Italy) (ARCA subdetector for cosmic neutrinos)
- **Sensitivity**: $1 - 10^4\ TeV$

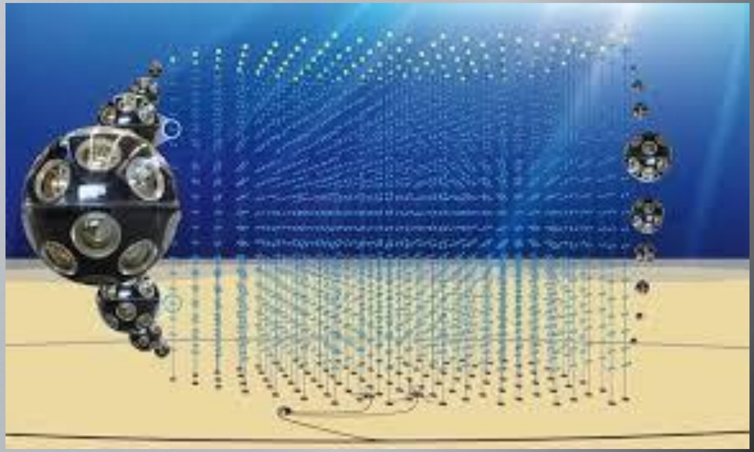

Detection

Neutrino observatories

- **IceCube** is the world's largest neutrino detector and one of the most important instruments for high-energy astrophysics.
- **Location**: 2.5 km below the ice, Amundsen-Scott South Pole Station, Antarctica
- **Sensitivity**: $0.01 - 10^4\ TeV$ (peak at $\sim 10\ TeV$ for muon neutrinos)

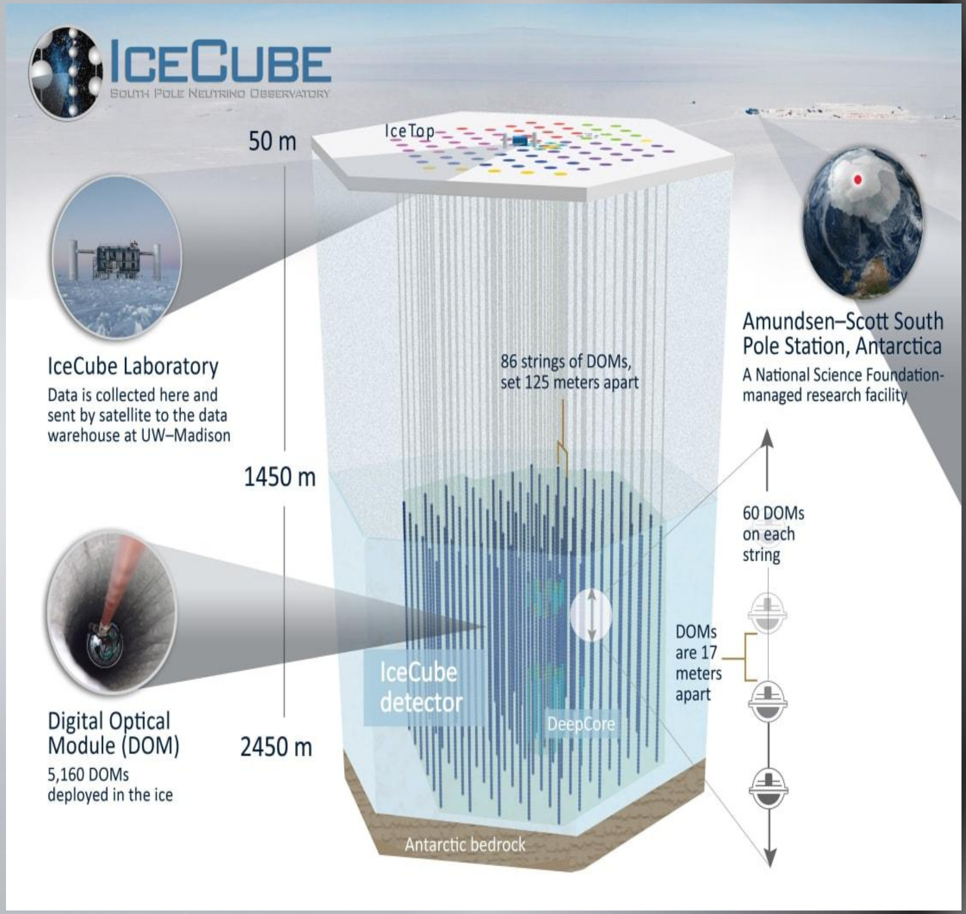

- **Upgrade: IceCube-Gen2** will extend the detector's volume to 8 km^3, increasing the detection rate of cosmic neutrinos by a factor of 10 and the sensitivity at the highest energies by 2 orders of magnitude

Detection

Very High-Energy γ-ray telescopes

- **MAGIC** is one of the most advanced instruments for observing VHE γ-rays from astrophysical sources
- **Location**: Roque de los Muchachos Observatory, La Palma, Canary Islands, Spain
- **Sensitivity**: $0.025 - 30\ TeV$

- **H.E.S.S.** is one of the world's leading ground-based gamma-ray observatories (upgraded to H.E.S.S II)
- **Location**: Khomas Highland, Namibia, southern Africa
- **Sensitivity**: $0.03 - 100\ TeV$

- **Upgrade: The Cherenkov Telescope Array (CTA)** is the next-generation ground-based γ-ray observatory designed to be the most sensitive instrument for VHE γ-ray astronomy to date. The sensitivity is expected to be 5–10× better than current MAGIC, H.E.S.S., etc. in the range $0.02 - 300\ TeV$

IV. Lepto-hadronic jet model

Relativistic Jets

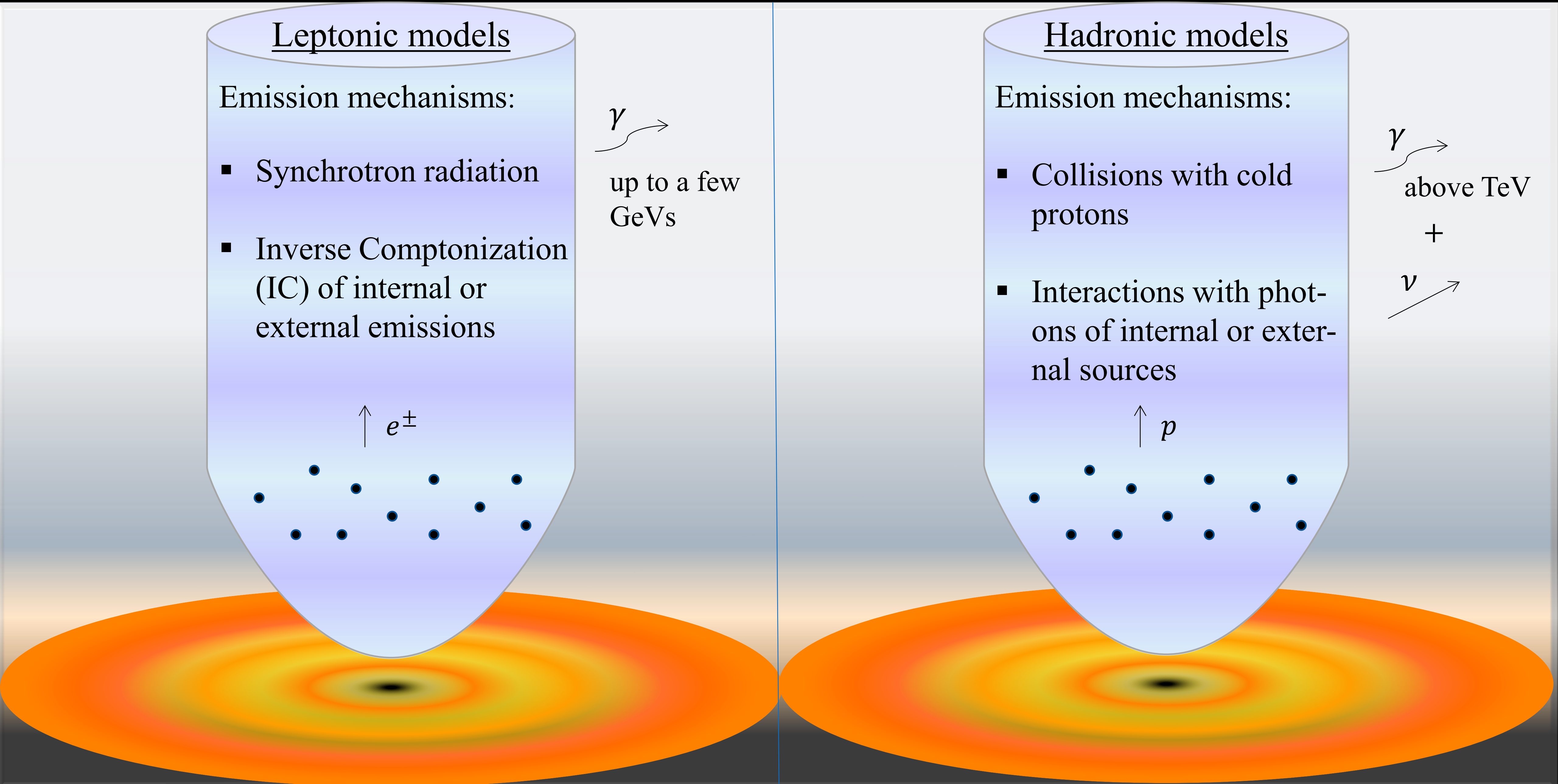

Fundamental assumptions of the jet model

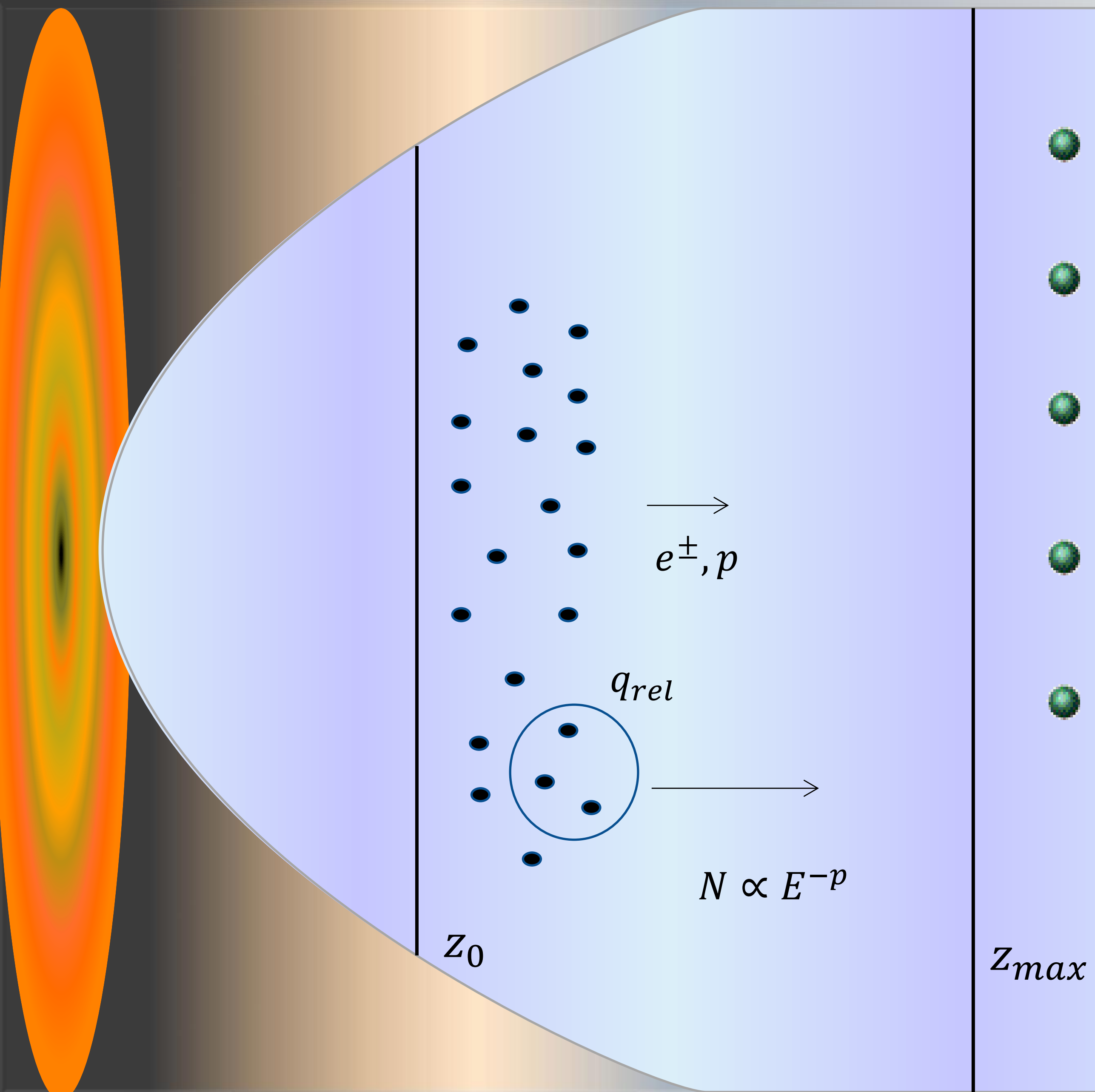

- $\rho_k = \rho_m \longrightarrow B(z) = \sqrt{8\pi\rho_k}$
- $L_k = 0.1 L_{Edd}$
- $L_p = a L_e$
- ${t_{acc}}^{-1} = \eta \frac{ceB}{E}$
- $L_{rel} = L_p + L_e = q_{rel} L_k$

$$\downarrow$$

$$\boxed{L_e = \frac{0.1 q_{rel} L_{Edd}}{a+1}}$$

Jet particle distributions

Transport equation

$$\frac{\partial N(E,z)b(E,z)}{\partial E} + t^{-1}N(E,z) = Q(E,z)$$

- $Q(E,z) = Q_0\left(\frac{z_0}{z}\right)^3 \frac{{\Gamma_b}^{-1}\left(E-\beta_b \cos i\sqrt{E^2-m^2c^4}\right)^{-2}}{\sqrt{sin^2 i+{\Gamma_b}^2\left(\cos i-\beta_b E/\sqrt{E^2-m^2c^4}\right)^2}}$
- Particle energy-loss rate: $b(E,z) = -Et_{loss}^{-1}$
- Cooling rates: $t_{loss}^{-1} = t_{sync}^{-1} + t_{pp}^{-1} + t_{ad}^{-1}$
- Particle number reduction rate: $t^{-1} = t_{esc}^{-1} + t_{dec}^{-1}$, $t_{esc}^{-1} \approx \frac{c}{z_{max}-z}$

$$N(E,z) = \frac{1}{|b(E)|}\int_E^{E_{max}} Q(E',z)e^{-\tau(E,E')}dE',$$

$$\tau(\mathrm{E},\mathrm{E}') = \int_{\mathrm{E}}^{\mathrm{E}'} \frac{\mathrm{dE}''t^{-1}}{|b(E'')|}$$

Leptonic & hadronic emission mechanisms

Synchrotron radiation

- $q_{syn} = \frac{\sqrt{3}e^3 B(z)}{hmc^2} x \int_x^{\infty} K_{\frac{5}{3}}(\zeta) d\zeta$

Inverse Compton spectrum

- $q_{IC} = \frac{3\sigma_T m^2 c^5}{4\gamma} \frac{n(\epsilon)}{\epsilon} [2f \ln f + (1+2f)(1-f) + F]\,,\; f = \frac{\mathrm{kE}}{4\epsilon\gamma^2}$

γ-rays & neutrinos from p-p collisions

- $Q_\gamma(E_\gamma, z) = cn(z) \int_{x_{min}}^{1} \frac{dx}{x} N_p\left(\frac{E_\gamma}{x}, z\right) F_\gamma\left(x, \frac{E_\gamma}{x}\right) \sigma_{pp}{}^{inel}\left(\frac{E_\gamma}{x}\right),\; x = \frac{E_\gamma}{E_p}$
- $Q_\nu = \int_E^{E_{max}} t^{-1}{}_{\pi,dec}(E_\pi) N_\pi(E_\pi, z) \frac{\Theta(1-r_\pi-y)}{E_\pi(1-r_\pi)} dE_\pi\,,\; y = \frac{E}{E_\pi}\,,\; r_\pi = \left(\frac{m_\mu}{m_\pi}\right)^2$

$$\boxed{L(E_\gamma) = \int_V E_\gamma Q\,(E_\gamma, z) d^3 r}$$

- $pp, p\gamma \to \pi^0, \pi^\pm$
  - $\pi^0 \to \gamma + \gamma$
  - $\pi^+ \to \mu^+ + \nu_\mu$
  - $\pi^- \to \mu^- + \bar{\nu}_\mu$

Photo-absorption due to γ-γ interactions

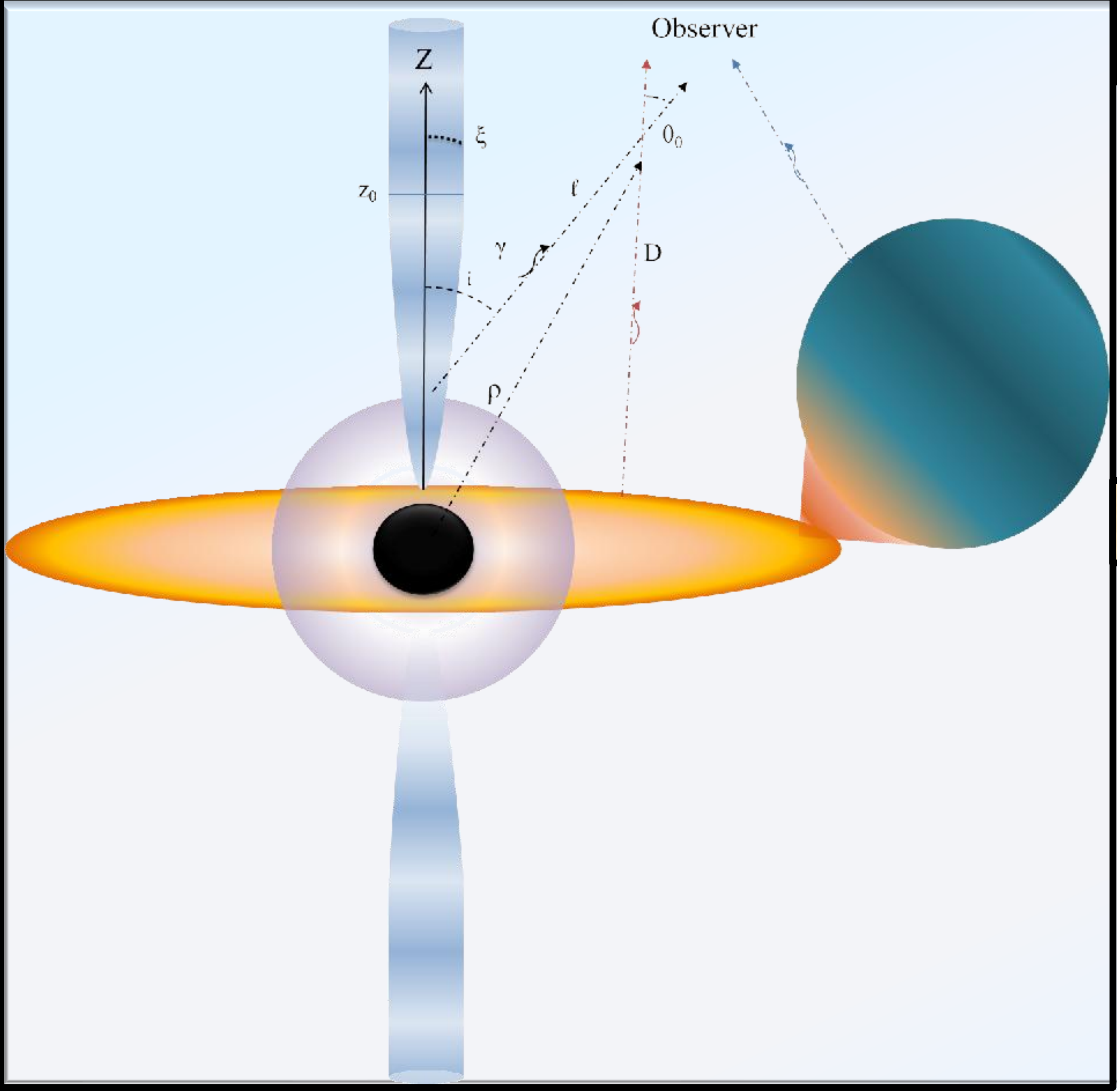

Accretion disk thermal emission

$$\tau_{disk} = \int_0^\infty \int_0^{2\pi} \int_{R_{in}}^{R_{out}} \int_{\epsilon_{min}}^\infty \frac{dn}{d\epsilon d\Omega}(1 - \cos\theta_0)\sigma_{\gamma\gamma}\frac{\rho\cos\omega}{D^3} RDRd\varphi\, d\epsilon dl$$

Stellar companion blackbody spectrum

$$\tau_{star} = \int_0^\infty \int_{\epsilon_{min}}^\infty \frac{dn_{ph}}{d\epsilon}(1 - \cos\theta_0)\sigma_{\gamma\gamma} d\epsilon dl$$

$$\epsilon_{min} = \frac{2m_e^2c^4}{E_\gamma(1 - \cos\theta_0)}$$

$$I = I_0 e^{-\tau}$$

Corona hybrid model

- We model the corona as a spherical region of radius R_c and optical depth τ_{cor} filled with thermal electrons described by a Maxwell-Juttner distribution

- In the thermal corona, there is an injection of a power-law distribution of non-thermal electrons

Thermal part

- $N_{th} = n_0 \dfrac{f_{MJ}(\gamma)}{m_e c^2}$
- $n_0 = \dfrac{\tau_{cor}}{\sigma_T R_c}$
- $f_{MJ}(\gamma) = \dfrac{\beta\gamma^2}{\vartheta K_2(1/\vartheta)} e^{-\gamma/\vartheta}$
- $\beta = \sqrt{\left(1 - \dfrac{1}{\gamma^2}\right)}\,, \qquad \gamma = \dfrac{E}{mc^2}$
- $\vartheta = \dfrac{k_B T}{m_e c^2}$

Non-thermal part

- $N_{nth} = \dfrac{n_0(-p_e+1)h_{cor}}{\gamma_{max}{}^{-p_e+1} - \gamma_{min}{}^{-p_e+1}} \dfrac{\gamma^{-p_e}}{m_e c^2}$
- $p_e \longrightarrow$ power-law index
- $h_{cor} \longrightarrow$ ratio of the non-thermal to thermal particles
- $\gamma_{min} \longrightarrow$ minimum energy of the injected electrons
- $\gamma_{max} \longrightarrow$ maximum energy of the injected electrons

μQSED Gauss-Legendre numerical integration

- Gauss–Legendre quadrature is a form of the Gaussian rule for integrating a function over the interval [−1, 1]

$$I = \int_{-1}^{1} f(x)dx \approx \sum_{i=1}^{n} w_i f(x_i)$$

n: number of sample points
x_i: integration points- roots of the nth Legendre polynomial $\longrightarrow$ increasing n $\longrightarrow$ higher accuracy
w_i: quadrature weights

- An interval modification to $[a, b]$ gives the integration approximation as

$$\int_a^b f(x)dx \approx \frac{b-a}{2} \sum_{i=1}^{n} w_i f\left(\frac{b-a}{2}\xi_i + \frac{a+b}{2}\right),$$

where $w_i = \frac{2}{(1-x_i)^2 P'_n(x_i)^2}$, $P_n(x)$: Legendre polynomials

- The μQSED code upgrades upon the numerical integration method by employing a segmental application of the Gauss-Legendre quadrature, increasing the accuracy and reducing the execution time of the computational process

- ☐ GL on the initial interval with $n = 100$ $\longrightarrow$ 172.8 min
- ☑ GL on multiple intervals with $n = 10$ $\longrightarrow$ 2.24 min

V. <u>Results</u>: High-energy γ-rays and neutrinos from XRBs

Lepto-hadronic distributions in the relativistic jets

Description	Parameter	Cyg X-1	LMC X-1
Jet's base	z_0 (cm)	8.43×10^8	3.10×10^8
Acceleration limit	z_{max} (cm)	42.15×10^8	15.50×10^8
Black Hole mass	M_{BH}	$14.8 M_\odot$	$10.91 M_\odot$
Distance from Earth	d (kpc)	1.86	48
Angle to the line-of-sight	θ (°)	27.1	36.38
Jet's half-opening angle	ξ (°)	1.5	3
Jet's bulk velocity	υ_b	0.6c	0.92c
Maximum proton energy	E_p^{max} (GeV)	6.09×10^6	1.04×10^7

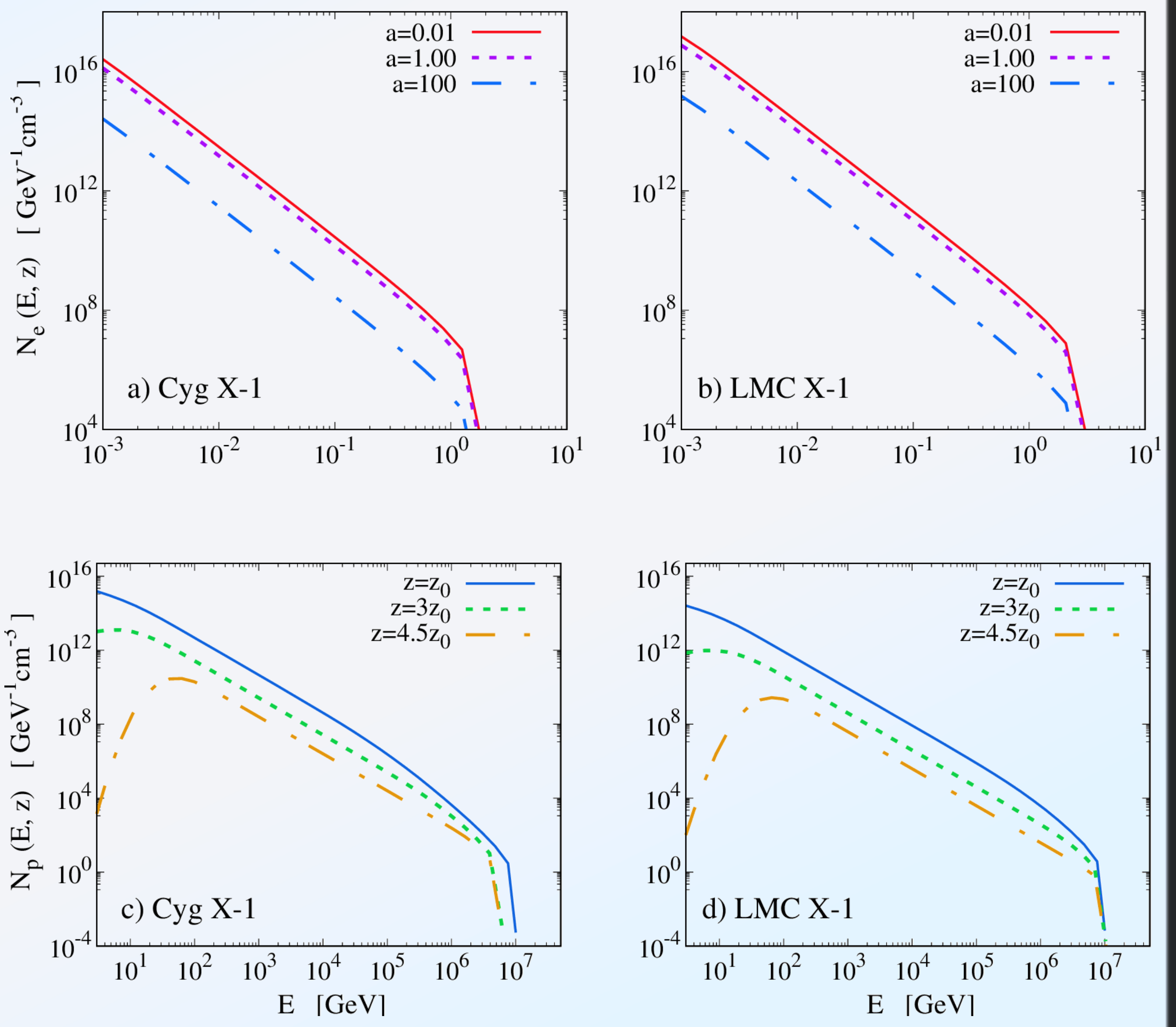

Pions & muons emerging from proton collisions

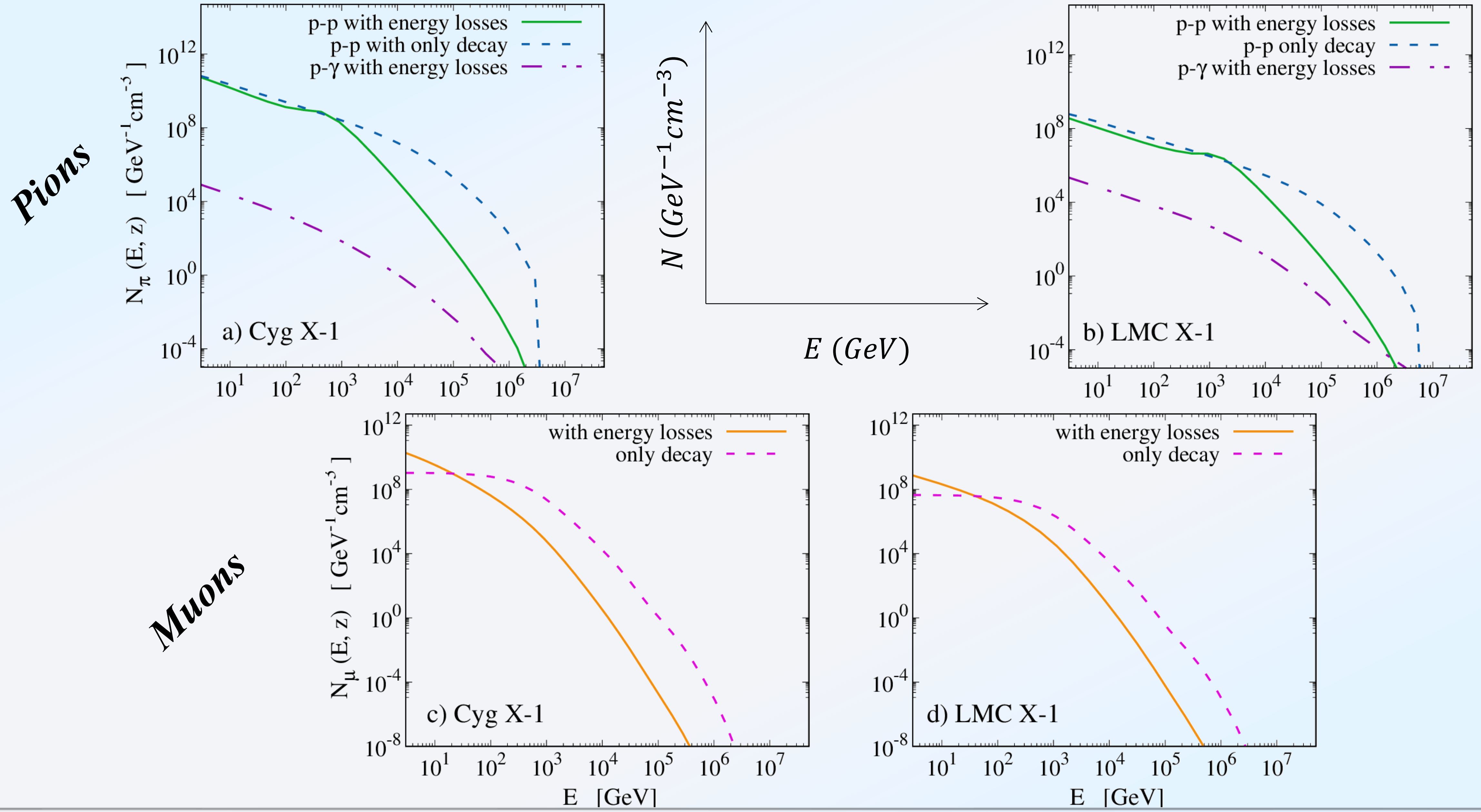

High-energy γ-ray emission from BH candidates

Parameter	Cyg X-1	SS 433	GRS 1915+105	Units
M_{BH}	21.2	15	12.4	$M_{\odot}$
M_{comp}	40.6	21	0.5	$M_{\odot}$
$Type$	O	A	K	-
d	2.22	5.5	8.6	kpc
i	27.51	78.8	60	°
P_{orb}	5.5998	13.082	33.85	$days$
$\dot{M}_{accr}$	10^{-8}	10^{-4}	10^{-8}	$M_{\odot} yr^{-1}$
L_{star}	3.5×10^{5}	3.16×10^{4}	10^{2}	$L_{\odot}$
T_{eff}	31138	8000	5000	K
s	3.65×10^{12}	5.37×10^{12}	7.19×10^{12}	cm
u_b	0.92	0.26	0.43	c
ξ	1.2	0.6	5	°
R_{out}	1.07×10^{12}	1.69×10^{12}	4.17×10^{12}	cm

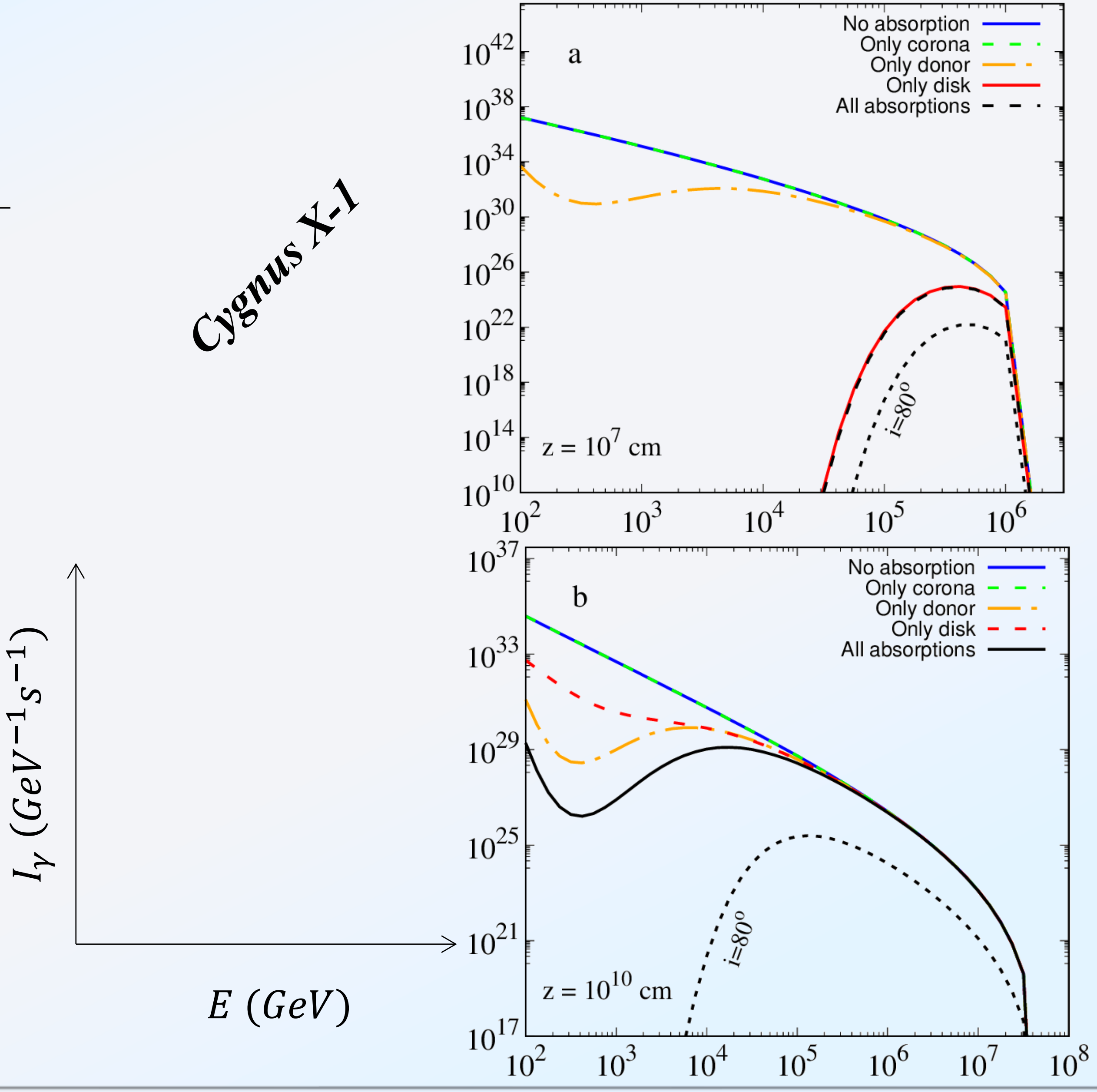

Papavasileiou Th., Kosmas O., Sinatkas I. 2023, *A&A*, **673**, A162

High-energy γ-ray emission from BH candidates

SS 433

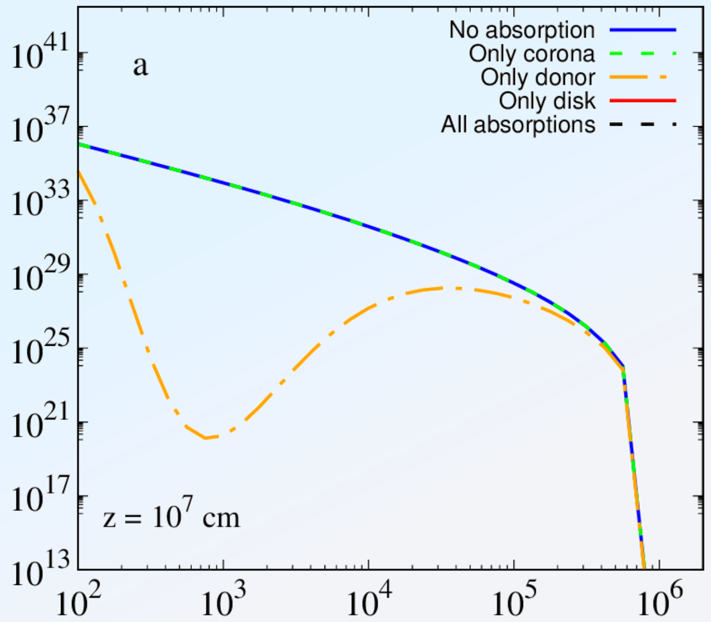

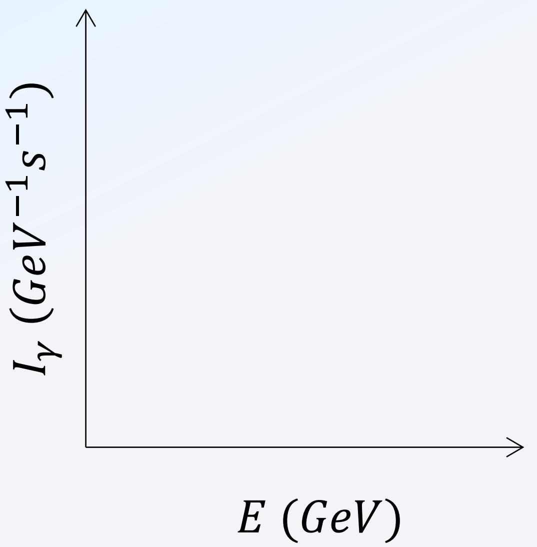

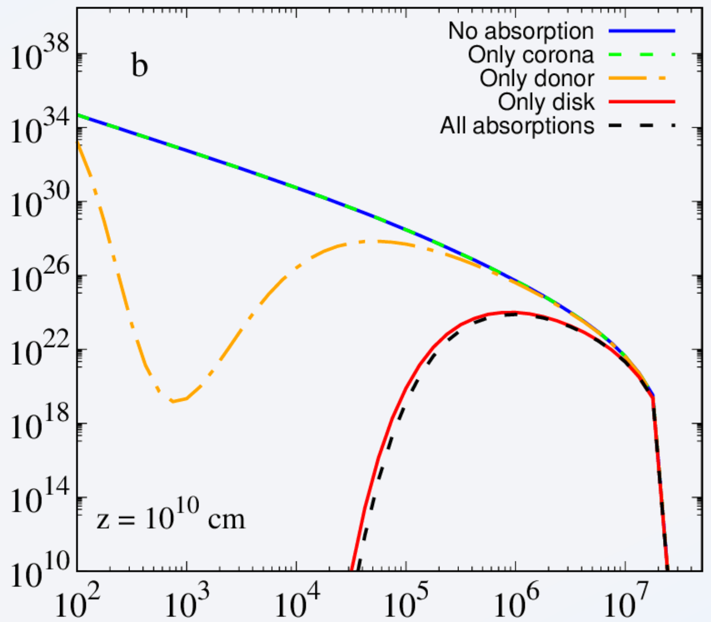

GRS 1915+105

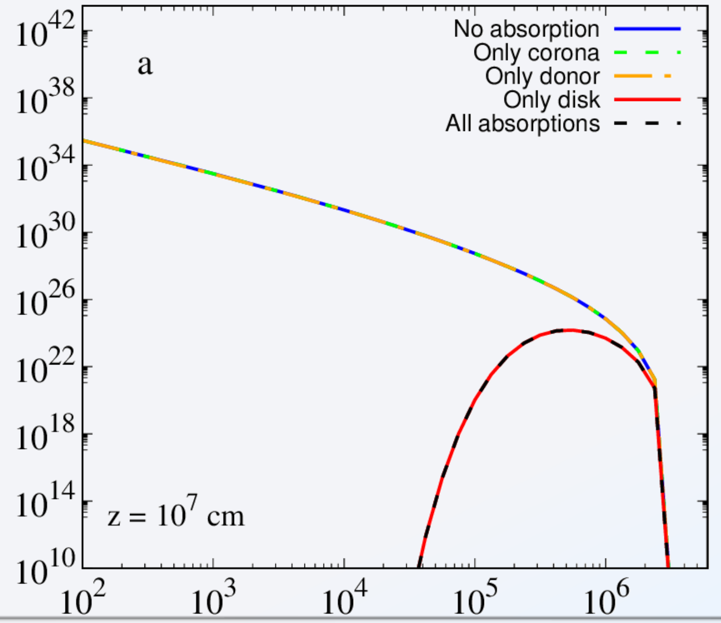

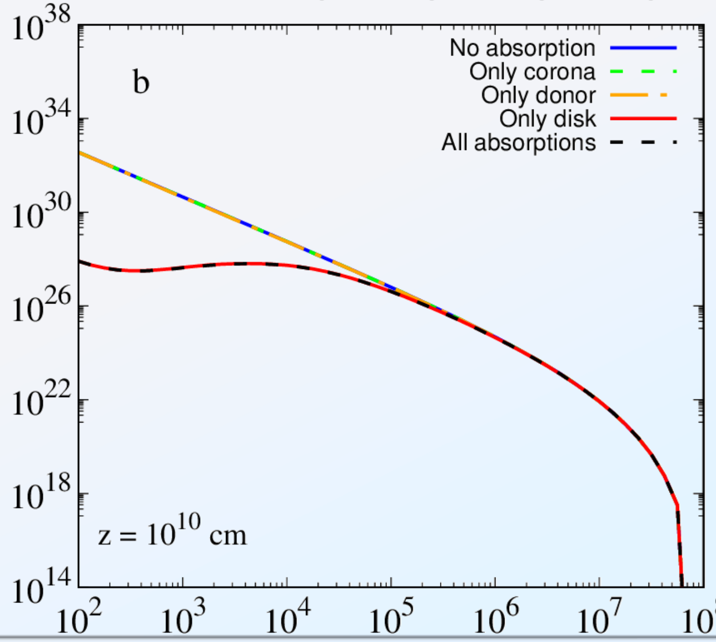

Papavasileiou Th., Kosmas O., Sinatkas I. 2023, *A&A*, **673**, A162

Absorbed photon fluxes from the expanded jet length

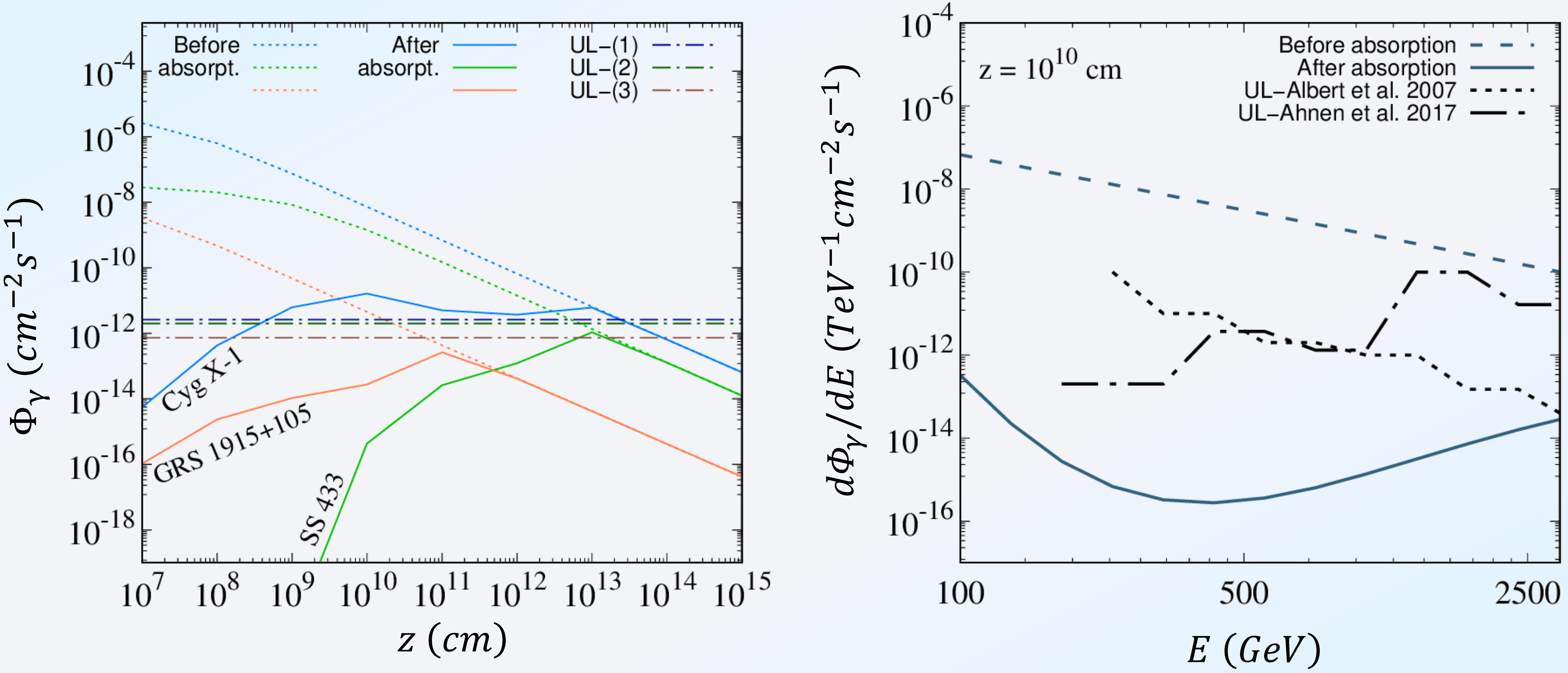

Papavasileiou Th., Kosmas O., Sinatkas I. 2023, *A&A*, **673**, A162

Expected TeV emissions from nearby XRBs

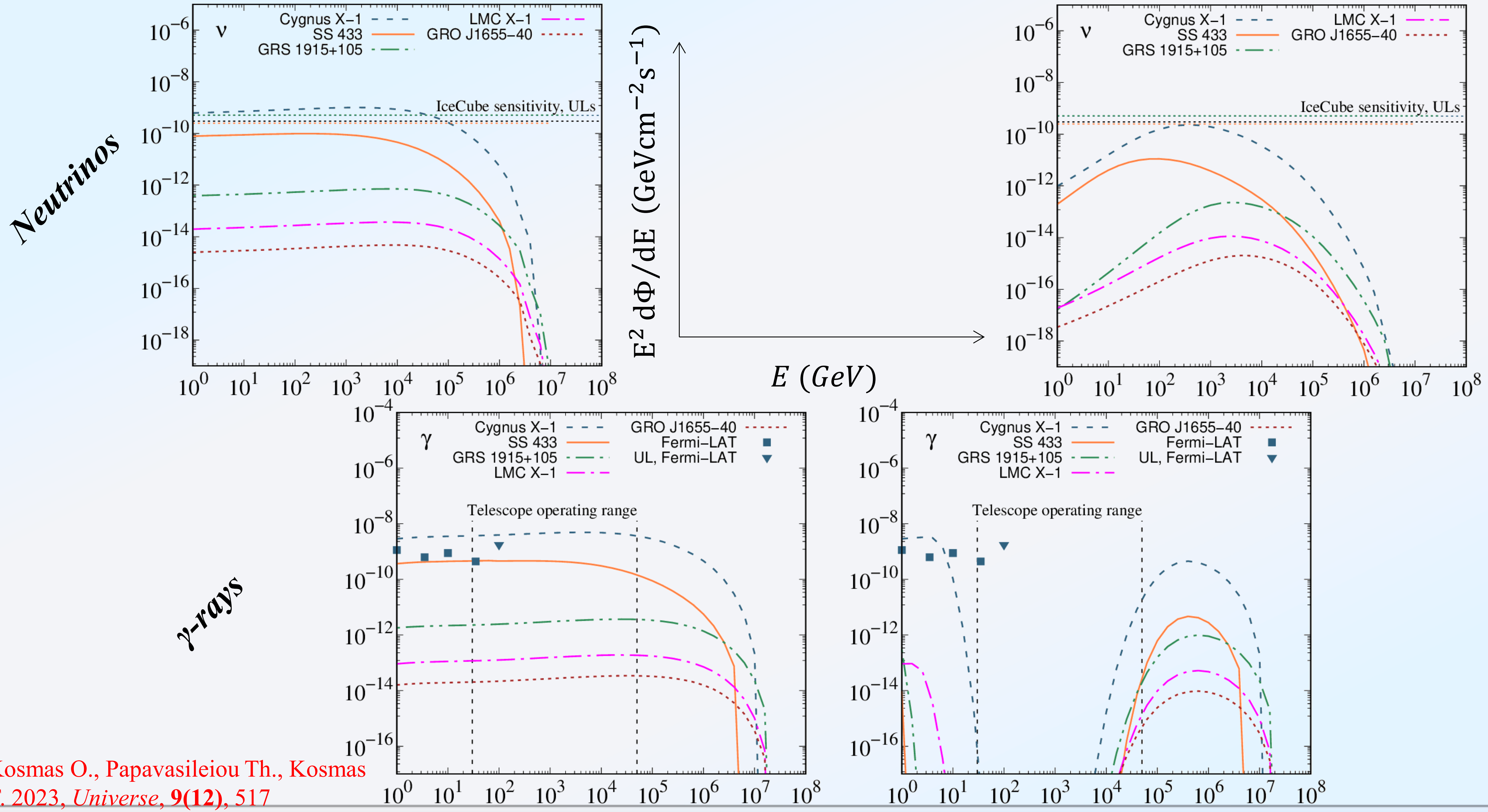

Kosmas O., Papavasileiou Th., Kosmas T. 2023, *Universe*, **9(12)**, 517

Parameter sensitivity in the lepto-hadronic jet model

$$\eta = \frac{E t_{acc}{}^{-1}}{ceB}$$

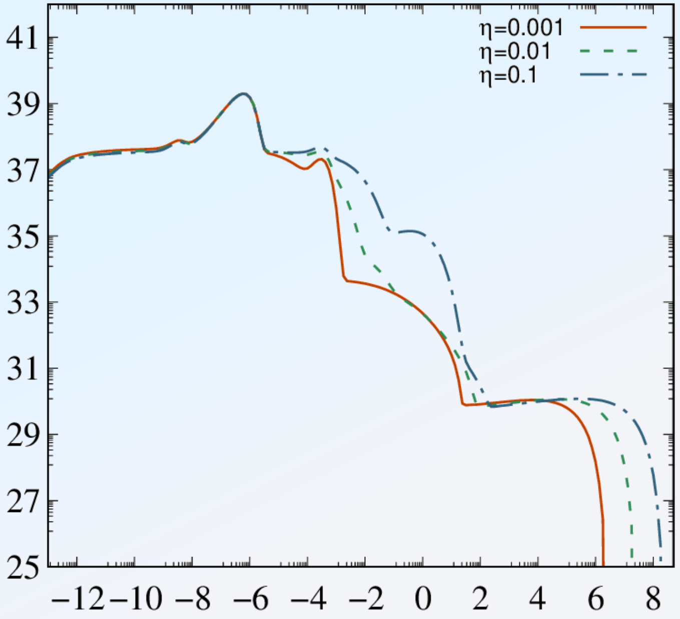

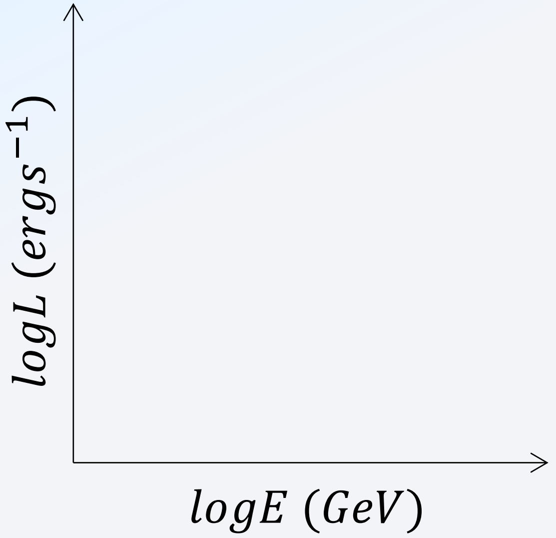

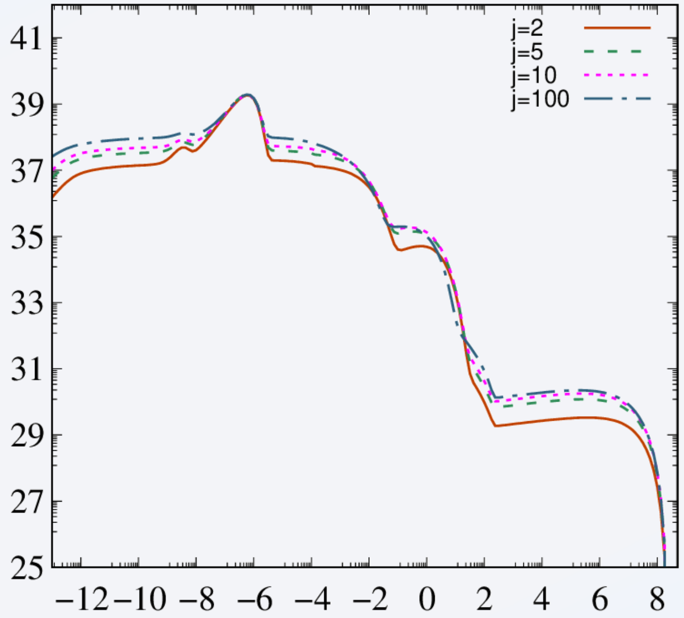

$$j = \frac{z_{max}}{z_0}$$

$$\alpha = \frac{L_p}{L_e}$$

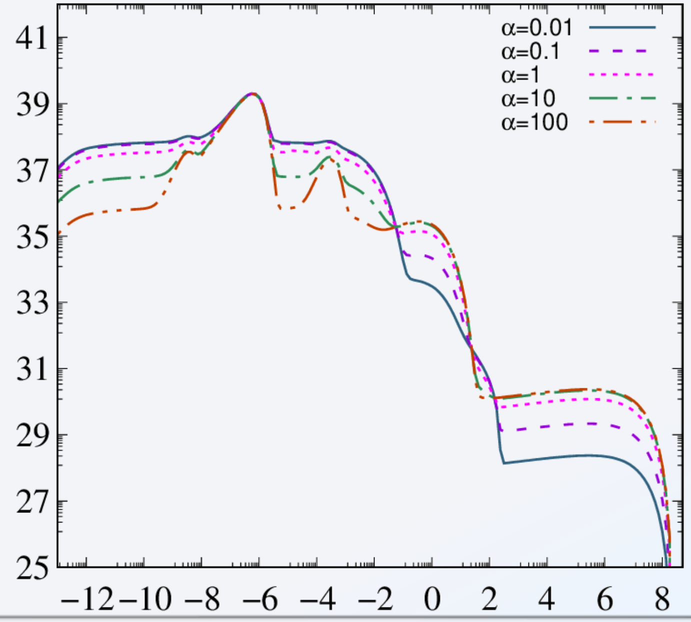

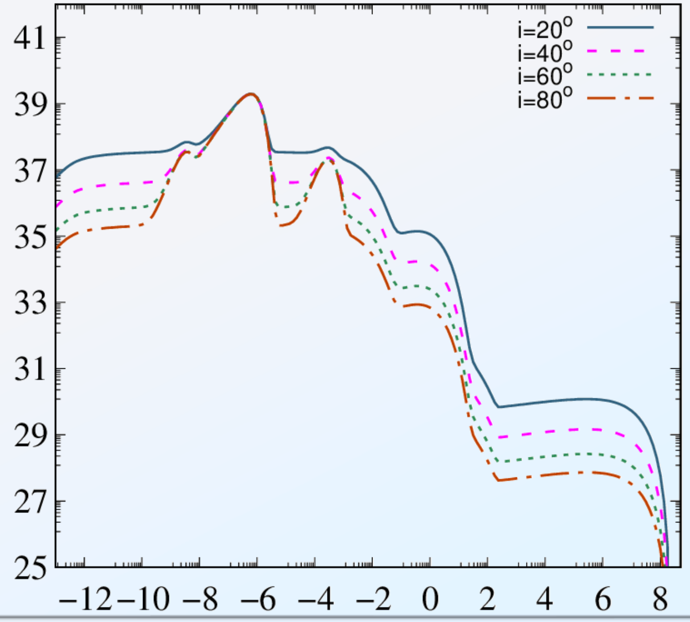

Angle to the line of sight

Papavasileiou Th., Kosmas O., Sinatkas I. 2023, *Universe*, **9(7)**, 312

Configuration of a sufficient particle accelerator

- Two cases of relativistic jet configurations:
  A. an efficient particle accelerator
  B. a radiatively-inefficient jet

Parameter	Case A	Case B
η	0.1	0.001
α	0.01	100
j	100	2
i	20°	80°

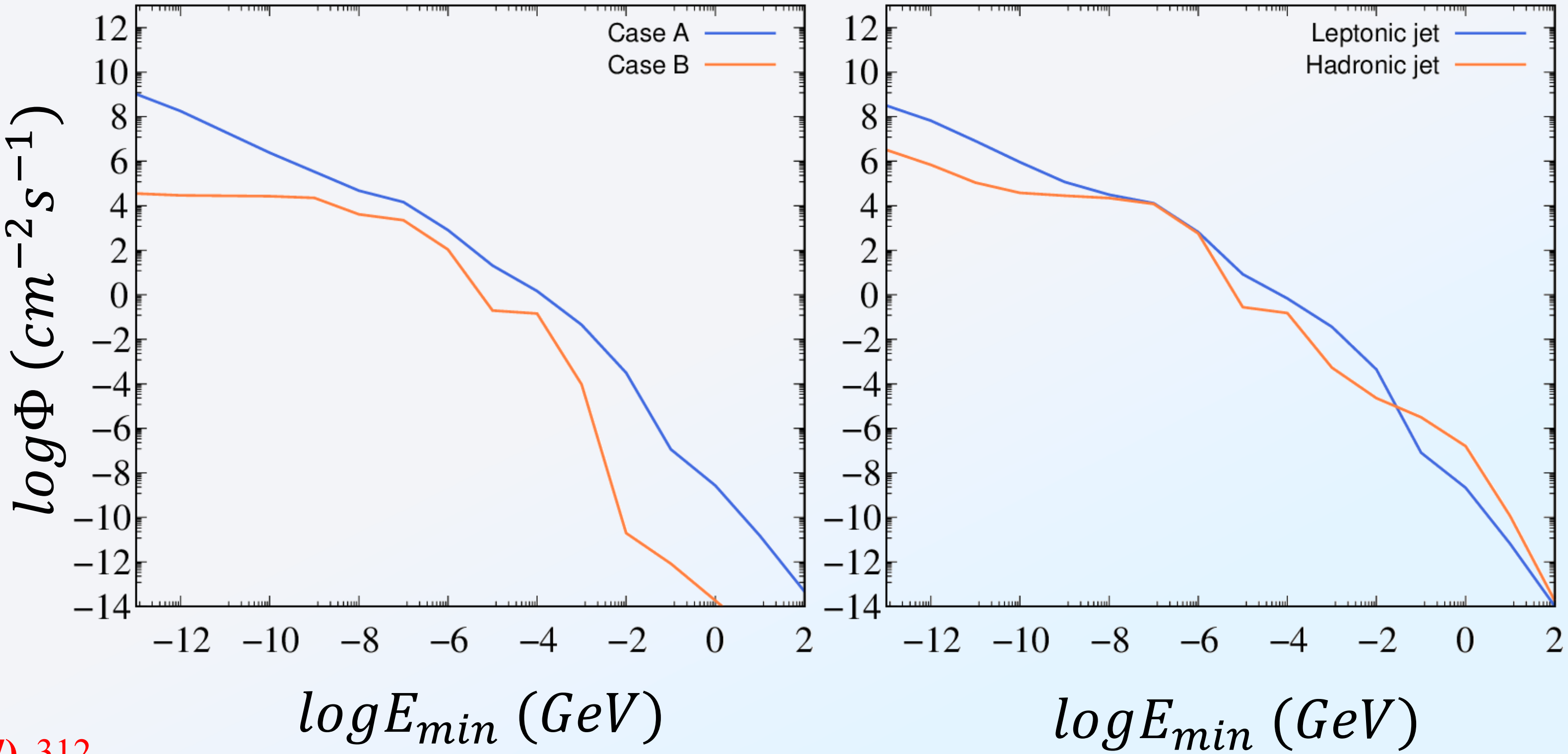

Papavasileiou Th., Kosmas O., Sinatkas I. 2023, *Universe*, **9(7)**, 312

VI. Results: A novel approach to calculating relativistic disk spectra

Kerr Metric Properties

- $r > R_{mb}$: marginally bound orbits
- $r > R_{ms}$: marginally stable orbits
- $R_g = \frac{GM_{bh}}{c^2} \rightarrow$ gravitational radius

- R_{ms} is called R_{ISCO} → Innermost Stable Circular Orbit
- $0 \leq \alpha_* \leq 1 \rightarrow$ dimensionless spin parameter
- In fact, $\alpha_* \leq 0.998$

Kerr metric in General Relativity

- ❑ $R_{mb} = \left(1 + \sqrt{1 \pm \alpha_*}\right)^2 R_g$
- ❑ $R_{ISCO} = \left(3 + Z_2 \pm \sqrt{(3 - Z_1)(2Z_2 + Z_1 + 3)}\right) R_g$
  - $Z_1 = 1 + (1 - \alpha_*^2)^{\frac{1}{3}}\left((1 + \alpha_*)^{\frac{1}{3}} + (1 - \alpha_*)^{\frac{1}{3}}\right)$
  - $Z_2 = \left({Z_1}^2 + 3{\alpha_*}^2\right)^{\frac{1}{2}}$

Non-rotating “Schwarzschild” black holes

❑ $\alpha_* = 0$ ❑ $R_{mb} = 4R_g$ ❑ $R_{ISCO} = 6R_g$

Rotating “Kerr” black holes

❑ −: co-rotation ❑ $R_g \leq R_{mb} \leq R_{ISCO} \leq 6R_g$

❑ +: counter-rotation ❑ $R_{mb} \leq 5.83R_g < R_{ISCO} \leq 9R_g$

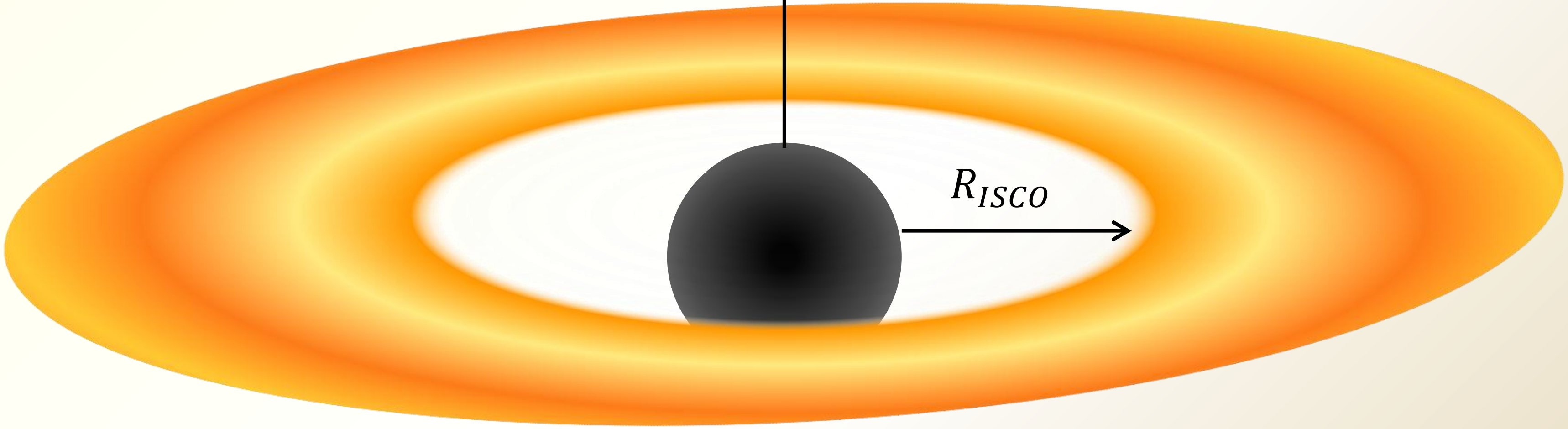

Kerr Pseudo-Newtonian Potential

- In most cases, a stationary compact object assumption is adopted in modeling the X-ray binary spectra
- The majority of stellar objects have angular momentum - Many black holes exhibit significant spin parameters
- The black hole's rotation could lead to a significant modification of the accretion disk's and the jet's energy output

Artemova potential

$$\mathrm{F_M} = \frac{\mathrm{G}M_{bh}}{{r_g}^2}\frac{1}{\bar{r}^{2-\beta}(\bar{r}-\bar{r}_h)^{\beta}} \longrightarrow$$

- $\bar{r}_h = 1 + \sqrt{1-{\alpha_*}^2}$
- $\beta = \frac{r_{in}}{r_h} - 1$

- $\bar{r} = r/r_g$, $\alpha_* \rightarrow$ dimensionless spin parameter, $r_{in} \rightarrow$ innermost disk boundary

Advantages

- ❑ Simple expression that reduces to Paczyński–Wiita potential for $\alpha_* = 0$
- ❑ Reproduces the Kerr metric properties such as R_{mb} and R_{ISCO} pretty accurately
- ❑ Particularly efficient for rapidly rotating black holes ($\alpha_* \approx 1$)
- ❑ Works for radii smaller than R_{ISCO}

Spin-dependent disk temperature profile

Newtonian

- $T_N(r) = T_o \left(\frac{1}{\bar{r}}\right)^{3/4} \left(1 - \sqrt{\frac{\bar{r}_{in}}{\bar{r}}}\right)^{1/4}$

Paczyński–Wiita

- $T_{PW}(r) = T_o \left[\frac{\bar{r}-2/3}{\bar{r}(\bar{r}-2)^3}\left(1 - \frac{3^{3/2}(\bar{r}-2)}{2^{1/2}\bar{r}^{3/2}}\right)\right]^{1/4}$

Artemova

- $T_A(r) = T_o \left(\frac{(3-\beta)(\bar{r}-\bar{r}_h)+\beta\bar{r}}{3\bar{r}^{3-\beta}(\bar{r}-\bar{r}_h)^{\beta+1}}\right)^{1/4} \left(1 - \frac{\mathcal{R}(\bar{r}_{in})}{\mathcal{R}(\bar{r})}\right)^{1/4}$
  - $\mathcal{R}(\bar{r}) = \left(\frac{\bar{r}^{\beta+1}}{(\bar{r}-\bar{r}_h)^{\beta}}\right)^{1/2}$

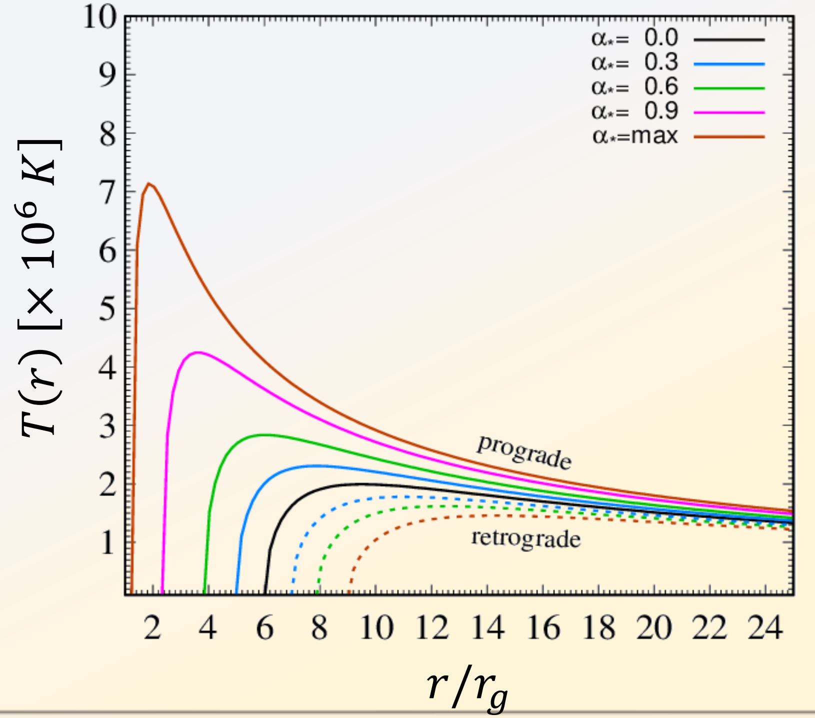

- $T_o = \left(\frac{3GM_{bh}\dot{M}}{8\pi\sigma r_g{}^3}\right)^{1/4}$, $\bar{r} = r/r_g$, $r_{in} \rightarrow$ disk inner edge

Papavasileiou Th., Kosmas O., Kosmas T. 2025, *A&A*, **693**, A75

Observed disk radiative efficiency

- Radiative Efficiency
  $\eta = L_{disk}/\dot{M}c^2$

- Shakura-Sunyaev
  $\eta_{obs} = 2\,\eta\cos\theta$

- Relativistic effects
  $\eta_{obs} = f(\theta, a)\eta(\alpha)$

- $f(\theta,\alpha) = A\cos\theta\,[1-(\sin\theta)^C]^B[1-E\,(\sin\theta)^F]^D$

A,B,C,D,E

↓

$$\Phi(\alpha_*) = \alpha + \beta x + \gamma x^2 + \delta x^3 + \varepsilon x^4 + \iota x^5 + \kappa x^6,$$
$$x = \log(1-\alpha_*)$$

Campitiello S. et al. 2018, *A&A*, **612**, A59

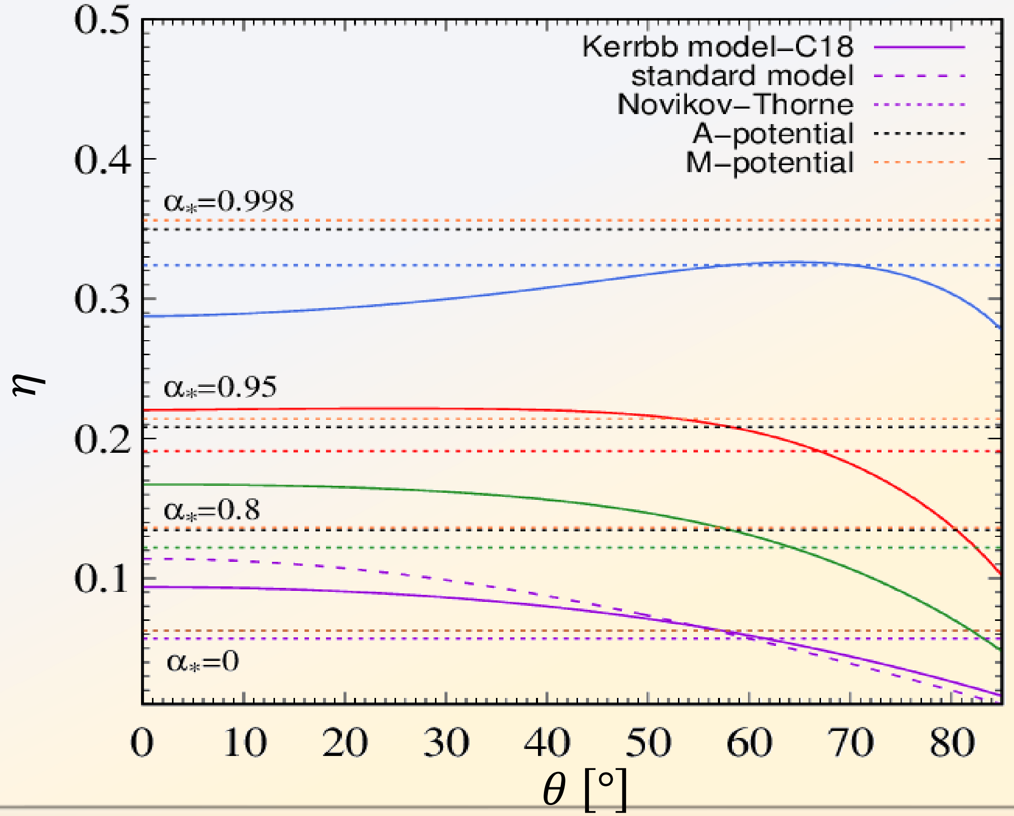

Papavasileiou Th., Kosmas O., Kosmas T. 2025, *A&A*, **693**, A75

Modification of the disk's inner boundary

Using the Artemova pseudo-potential…

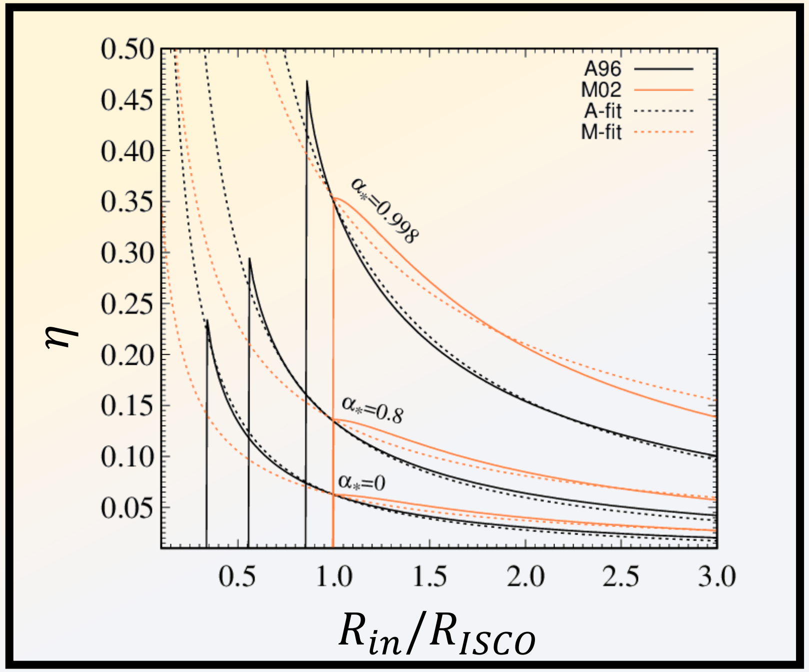

- Fitting the radiative efficiency

$$\eta(R_{in}) = \eta(R_{ISCO})\left(\frac{R_{in}}{R_{ISCO}}\right)^{-1,17}$$

- Equating with the relativistic efficiency

$$\eta(R_{in})(2\cos\theta) = f(\theta, a)\eta(\alpha)$$

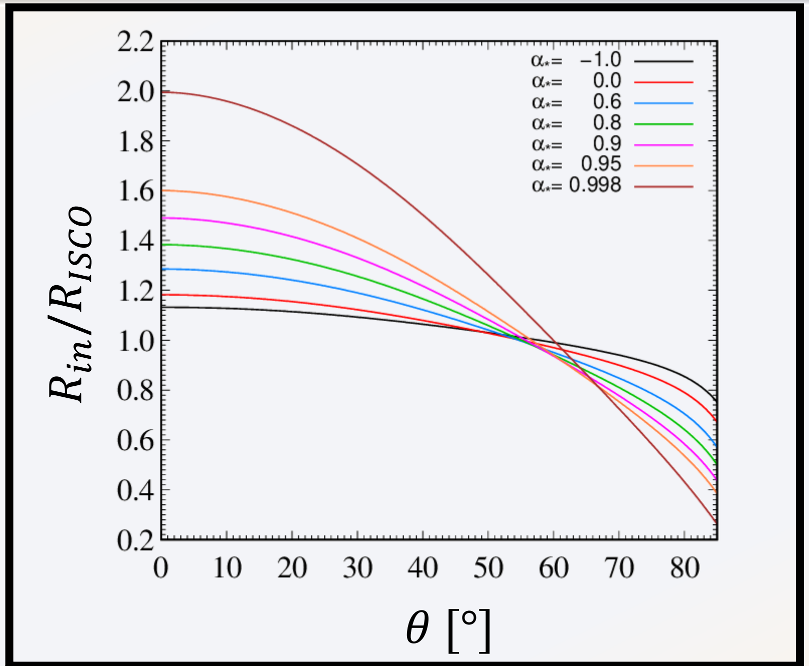

- Disk radius modification

$$R_{in} = \left(\frac{2\cos\theta}{f(\theta, \alpha)}\right)^{\frac{1}{1,17}} R_{ISCO}$$

Papavasileiou Th., Kosmas O., Kosmas T. 2025, *A&A*, **693**, A75

How does our approach compare to General Relativity?

- $\theta = 60^{\circ}$ → The PN solution is accurate → $\mathrm{R}_{in} \cong R_{ISCO}$
- $\theta > 60^{\circ}$ → The PN solution underestimates the observed total luminosity → $\mathrm{R}_{in} < R_{ISCO}$
- $\theta < 60^{\circ}$ → The PN solution overestimates the observed total luminosity → $\mathrm{R}_{in} > R_{ISCO}$

PN comparison

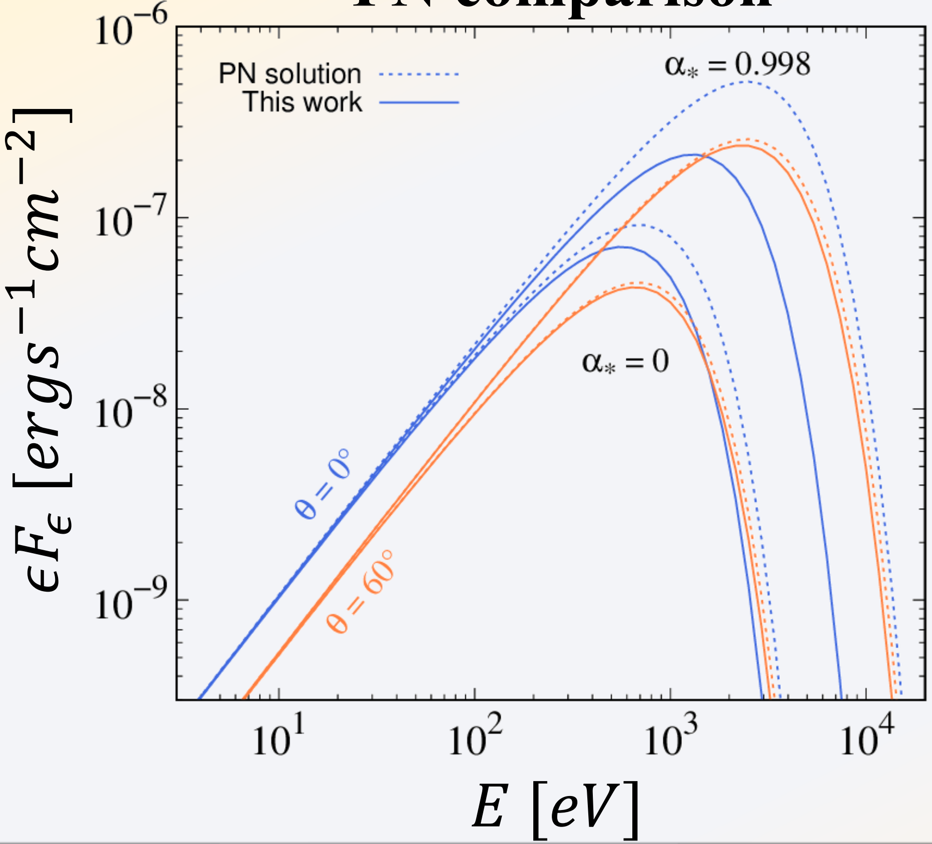

GR comparison

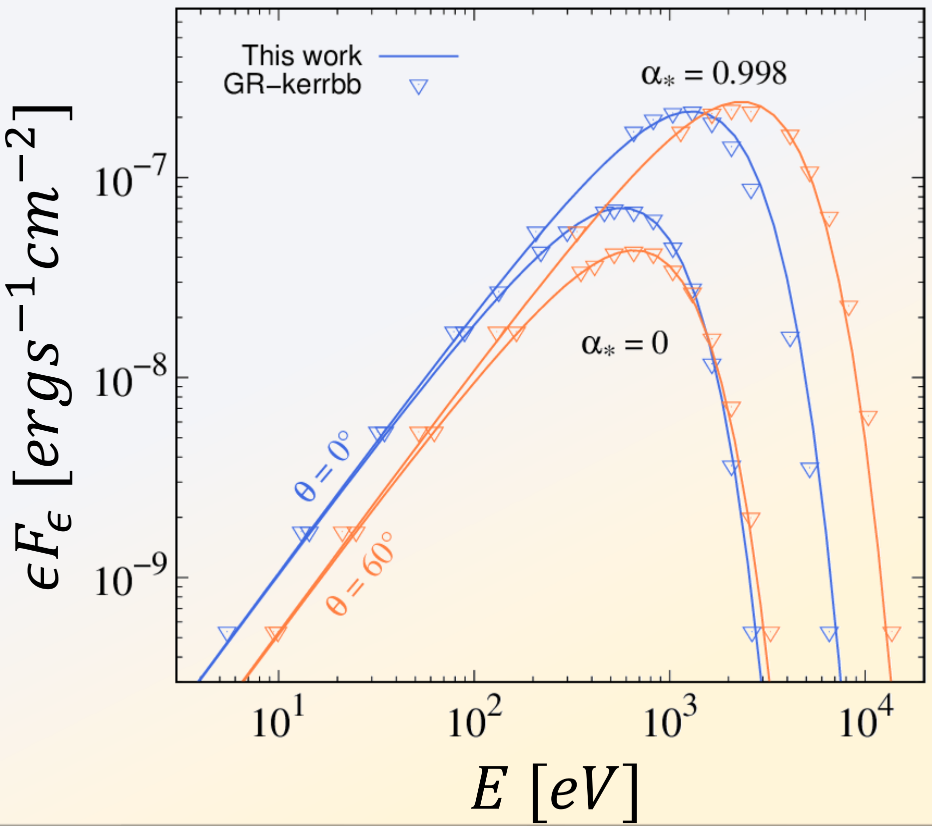

Papavasileiou Th., Kosmas O., Kosmas T. 2025, *A&A*, **693**, A75

Error margin & deviation from General Relativity

❑ Three sources of error in this approach

- The intrinsic error margin of the analytic function $f(\theta, a)$ $\rightarrow$ $< \mathbf{1\%}$
- The error due to the PN potential adoption $\rightarrow$ $< \mathbf{8-9\%}$
- The error due to the deviation caused by the choice of the p = 1.17 index

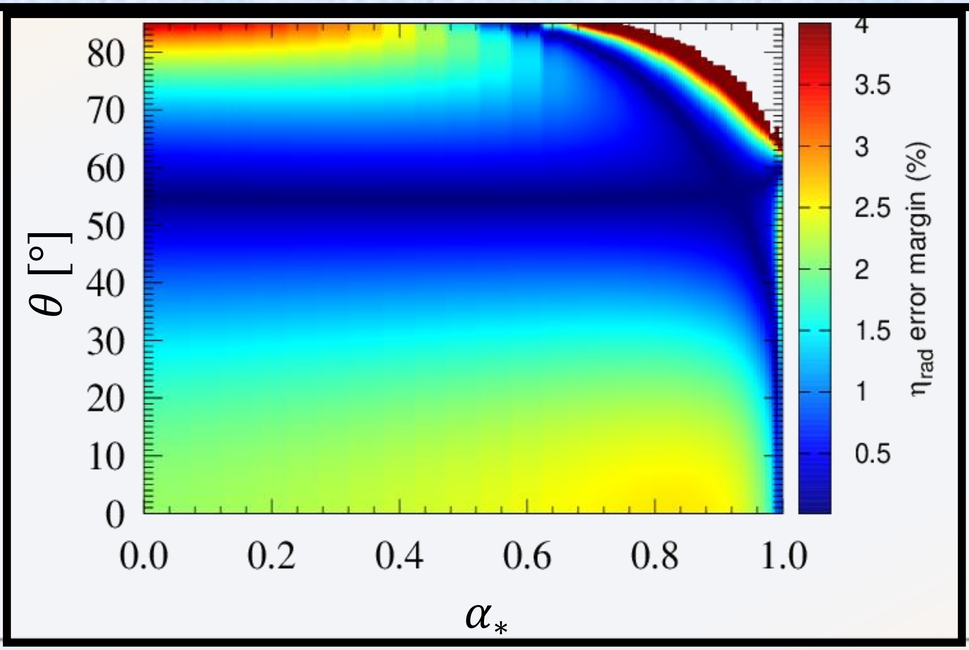

✓ Solution

- Insignificant
- Introduce the factor k as $R'_{ISCO} = kR_{ISCO}$, with k ≈ 1.075 on average
- More suitable choice of p = 1.05−1.2 for a specific spin-angle combination

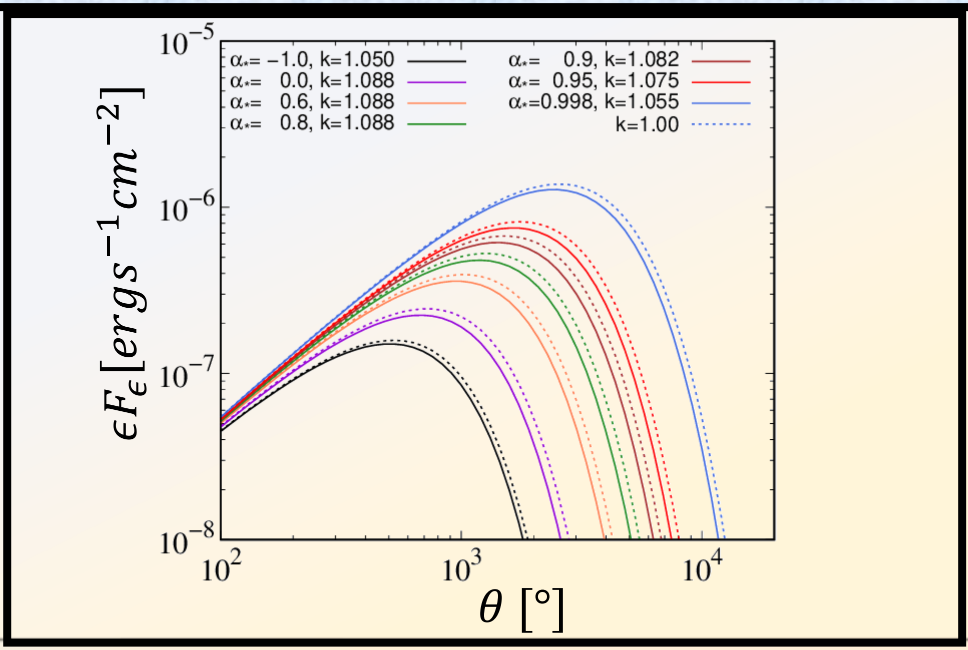

Papavasileiou Th., Kosmas O., Kosmas T. 2025, *A&A*, **693**, A75

Fitting the Cygnus X-1 spectra

Accretion disk - Corona		
Parameter	High/Soft	Hard/Low
R_{in}/R_{ISCO}	1	20
$\dot{m}$	0.007	0.004
R_{cor}/R_g	20	60
T_{cor} [keV]	50	150
τ_{cor}	0.29	0.50
p	4.9	1.8
γ_{min}	1.8	1.7
γ_{max}	>20	>26
h	0.050	0.294
Relativistic jet		
z_i [cm]		3×10^8
z_f/z_i		3
q_{rel}		3×10^{-5}
η_{acc}		0.15
L_p/L_e		0.009
β_{jet}		0.92
ξ [°]		1.2

Parameter	M_{bh}	M_{donor}	d	θ	P_{orb}	a_*	L_{star}	T_{star}
Cygnus X-1	21.2	40.6	2.22	60	5.5998	0.97	3.95×10^5	31138
Units	$M_\odot$	$M_\odot$	kpc	°	$days$	-	$L_\odot$	K

High/soft state

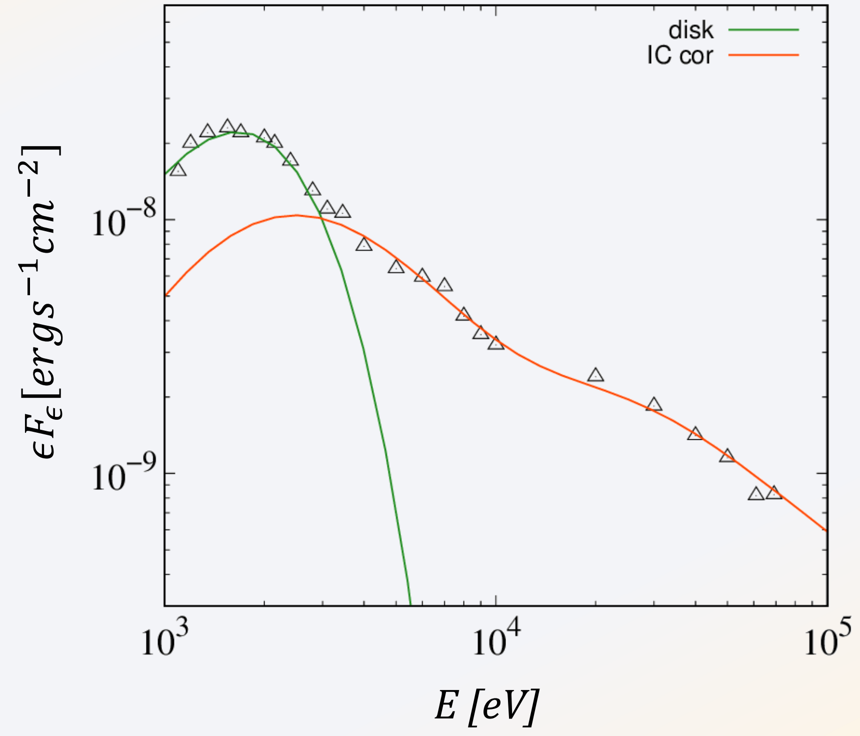

Hard/low state

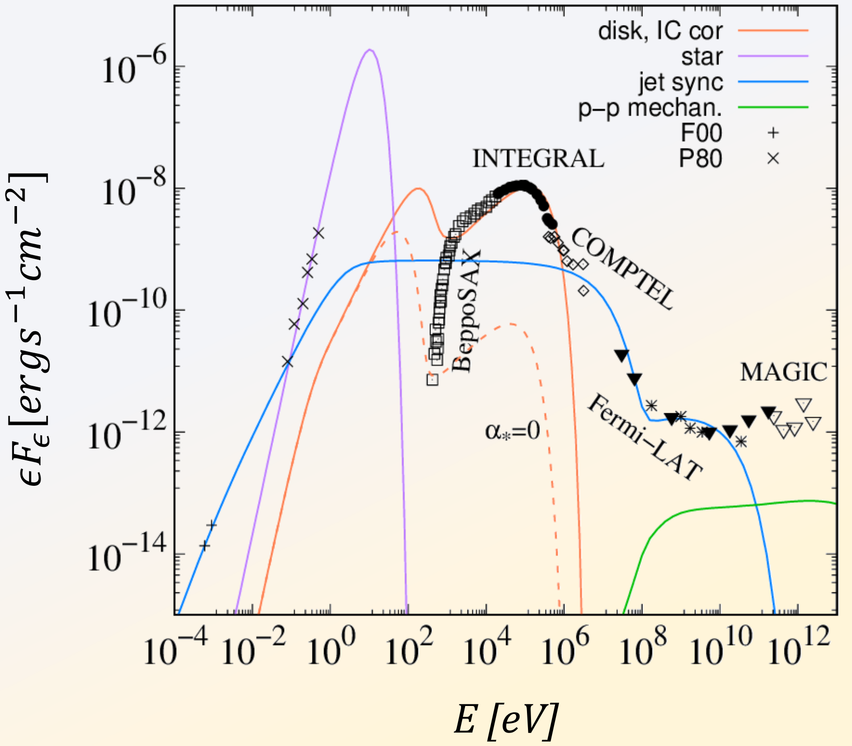

Papavasileiou Th., Kosmas O., Kosmas T. 2025, *A&A*, **693**, A75

VII. Summary & Conclusions

Conclusions I

- Very low prospects of neutrino detection, except Cygnus X-1 in the 0.1-1 TeV range → Particle cooling due to synchrotron emission and inelastic collisions below 100 GeV

- The jet γ-ray fluxes are absorbed in the 100 GeV - 10 TeV range → most gamma-ray telescopes operation → lack of high-energy γ-ray spectra from XRB sources

- Lack of high-energy γ-ray emission → inefficient proton acceleration and inelastic collisions at higher jet grids → reduction of γ-ray photon production

- Increase in broadband emission from radio to VHE gamma-rays when:
  - $i < 20°$
  - $a \ll 1$
  - $z_0 > 10^{11}\ cm$
  - $z_{max} \approx 10 z_0$

- We fit the observational data of Cygnus X-1 during the high/soft and the hard/low state:
  - High/soft → Blackbody + IC due to a thermal/non-thermal corona
  - Hard/low → Sync from lepto-hadrons + (Blackbody with $R_{in} > R_{isco}$ + IC) + p-p

Conclusions II

Relativistic disk spectra

- ✓ light-bending
- ✓ Doppler beaming
- ✓ gravitational redshift
- ✓ self-irradiation

KERRBB

Thin disk
+
Novikov-Thorne correction
+
Ray-tracing technique

- $T_A(r) = T_o\left(\frac{(3-\beta)(\bar{r}-\bar{r}_h)+\beta\bar{r}}{3\bar{r}^{3-\beta}(\bar{r}-\bar{r}_h)^{\beta+1}}\right)^{\frac{1}{4}}\left(1-\frac{\mathcal{R}(\bar{r}_{in})}{\mathcal{R}(\bar{r})}\right)^{\frac{1}{4}}, \ \mathcal{R}(\bar{r}) = \left(\frac{\bar{r}^{\beta+1}}{(\bar{r}-\bar{r}_h{}^{\beta})}\right)^{1/2}$
- $R_{in} = \left(\frac{2\cos\theta}{f(\theta,\alpha)}\right)^{\frac{1}{1{,}17}} R_{ISCO}$
- Error → < 3.5 %

THIS WORK

Standard model
+
$T_{PW}(r) \rightarrow T_A(r, a_*)$
+
$R_{ISCO} \rightarrow R_{in}(a_*, \theta)$

References

1. Bosch-Ramon, V. , Romero, G. E. & Paredes, J. M. 2006, *A&A*, **447**, 263
2. Reynoso, M. M. & Romero, G. E. 2009, *A&A*, **493**, 11.
3. Reynoso, M. M. & Carulli, A. M. 2019, *APh*, **109**, 25
4. Kelner, S. R., Aharonian, F. A., & Bugayov, V. V. 2006, *PRD*, **74**, 034018
5. Papavasileiou, Th. V., Kosmas, O., & Kosmas, T. S. 2025, *A&A*, **693**, A75
6. Papavasileiou, Th. V., Kosmas, O. T., & Sinatkas, I. 2023, *A&A*, **673**, A162
7. Papavasileiou, Th. V., Kosmas, O., & Sinatkas, I. 2023, *Universe*, **9(7)**, 312
8. Kosmas, O. & Smponias, T. 2018, *AdHEP*, **9602960**
9. Cerutti, B., Dubus, G., Malzac, J., et al. 2011, *A&A*, **529**, A120
10. Ahnen, M. L. et al. 2018, *A&A*, **612**, A14
11. Malyshev, D., Zdziarski, A. A., & Chernyakova, M. 2013, *MNRAS*, **434**, 2380
12. Miller-Jones, J. C. A. et al. 2021, *Science*, **371**, 1046
13. Tetarenko, A. J. et al. 2019, *MNRAS*, **484**, 2987
14. Campitiello, S., Ghisellini, G., Sbarrato, T., & Calderone, G. 2018, *A&A,* **612**, A59

Acknowledgement

- Prof. Ioannis Sinatkas, Department of Informatics, University of Western Macedonia
- Dr. Odysseas Kosmas, Department of Physics, University of Ioannina
- Prof. Theocharis Kosmas, Department of Physics, University of Ioannina
- Mr. Athanasios Gkrepis, Department of Informatics, University of Western Macedonia

UNIVERSITY OF
WESTERN MACEDONIA

University of Ioannina

OPRA

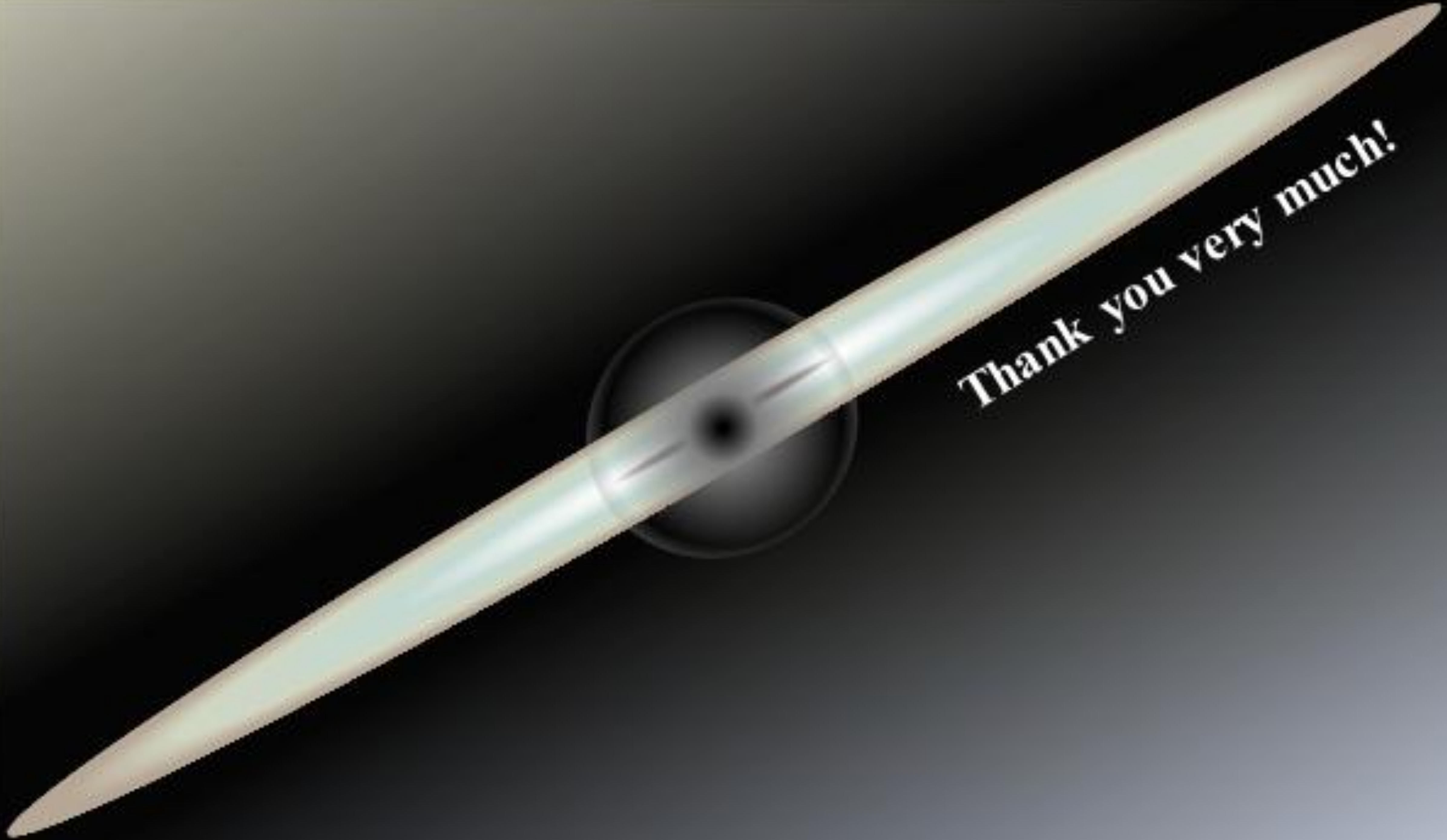

Thank you very much!